Chapter 6
Atmospheric and Ascent Flight

Now that we know the technical and physical properties of a rocket and the general equation of motion, which governs its flight, we are ready for a mission to the planets in our solar system. Before we investigate the rocket's motion in interplanetary space, it first has to ascent in Earth's gravitational field through the atmosphere. As will be shown later, ascent and reentry are subject to identical physical laws treated by the science called *flight mechanics*. The difference between the two is that reentry is powerless and the initial conditions of both mission phases are drastically different. This is why the problems we have to deal with are much different, and we therefore devote a chapter of its own (Chap. 10) to reentry after we consider orbital motion (Chap. 7), orbital maneuvering (Chap. 8), and come back from an interplanetary journey (Chap. 9). For ascent and for reentry, the properties of Earth's atmosphere are crucial. This is why we will first examine here the atmosphere's condition (Sect. 6.1) and the general laws of motion through the atmosphere (Sect. 6.2). Only after that shall we go (Sects. 6.3 and 6.4) into the specifics of how to optimize an ascent into space.

6.1 Earth's Atmosphere

From a space flight point of view, the atmosphere plays an important role during ascent, Earth orbiting, and reentry. First, because of the aerodynamics at lower altitudes and, second, because it also impacts low Earth orbits due to the residual atmospheric drag at high altitudes. To determine these influences quantitatively, we have to derive expressions that describe the density distribution in the atmosphere as a function of altitude.

U. Walter, *Astronautics*, https://doi.org/10.1007/978-3-319-74373-8_6

6.1.1 Density Master Equation

It is well known that atmospheric pressure, starting from sea level, decreases with increasing altitudes. To describe its quantitative dependency in mathematical terms, we first imagine that the atmosphere is a stack of infinitesimally thin layers with thickness ds (see Fig. 6.1). Without loss of generality, we assume a layer of having a surface A of arbitrary size. The volume of the layer is then $A \cdot ds$ and the mass of air within it is $dm = \rho A \cdot ds$, where ρ is the atmospheric mass density. The additional infinitesimal pressure it generates onto the ones below is the weight force per square unit

$$dp = d\left(\frac{mg}{A}\right) = \frac{g}{A} dm = \frac{g}{A} d(\rho A s) = \rho g \cdot ds$$

Here s measures the height against increasing pressure, which is in the same direction as the increase in gravitational force. But atmospheric pressure is usually given as a function of altitude h relative to sea level, i.e., in the opposite direction. So $ds = -dh$. Therefore we find for the pressure change of the atmospheric pressure

$$\frac{dp}{dh} = -\rho g(h) \tag{6.1.1}$$

where we have taken into account that with the gravitational acceleration g decreases with altitude according to

$$g(h) = g_0 \frac{R_\oplus^2}{r^2} = g_0 \frac{R_\oplus^2}{(R_\oplus + h)^2}$$

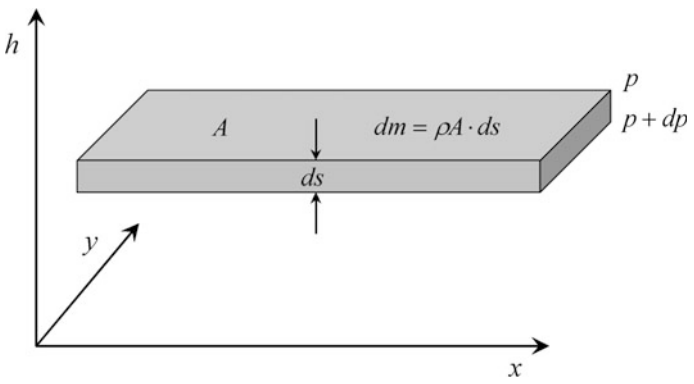

Fig. 6.1 Characteristics of an infinitesimally thin atmospheric layer

with $g_0 = 9.798\ \mathrm{m\ s^{-2}}$ and $R_\oplus = 6378.136$ km the Earth's radius. We now need to know how a gas behaves under external pressure. Earth's atmosphere can be described in a very good approximation by the ideal gas law (cf. Eq. (4.1.1))

$$p = \rho R_s T \quad \textbf{ideal gas law} \tag{6.1.2}$$

where T is the layer's temperature and

$$R_s = \frac{R}{M_{air}} = 286.91\ \frac{\mathrm{J}}{\mathrm{K \cdot kg}} \quad \begin{matrix}\textbf{specific gas constant} \\ \textbf{of standard atmosphere}\end{matrix}$$

Strictly speaking, R_s holds only for the standard atmosphere, i.e., for the standard molecular composition. As we will see, only particular parts of the atmosphere fulfill this requirement. We now differentiate Eq. (6.1.2) with regard to the altitude h. Because ρ and T depend on h, this yields with Eq. (6.1.1)

$$\frac{dp}{dh} = \frac{d\rho}{dh} R_s T + \rho R_s \frac{dT}{dh} = -\rho g(h)$$

From this follows that

$$\frac{d\rho}{\rho} + \frac{dT}{T} = -\frac{g(h) \cdot dh}{R_s T(h)} \tag{6.1.3}$$

This equation is the master equation to calculate the density function $\rho(h)$ for a given $T(h)$. By applying Eq. (6.1.2) $p(h)$ may then be derived. So all we need to know is the temperature profile $T(h)$. This is depicted in Fig. 6.2.

6.1.2 *Atmospheric Structure*

In terms of modeling, the atmosphere can be divided in two quite different zones:

1. The so-called **homosphere** extends to an altitude of roughly 120 km and includes the troposphere, stratosphere, mesosphere, and part of the thermosphere. The name derives from the fact that it is constituted by a homogeneous mixture of the standard atmospheric components, and therefore $R_s = const$. Although overall the homosphere shows only modest variations in temperature, each layer behaves meteorologically differently due to their different temperature gradients (see Fig. 6.2).
2. The so-called **heterosphere** extends above about 120 km and includes most of the thermosphere and exosphere (see Fig. 6.2). As its name indicates, the molecular constituents are heterogeneous with height and become partly ionized, all of which results in $R_s \neq const$. Its temperature deviates significantly

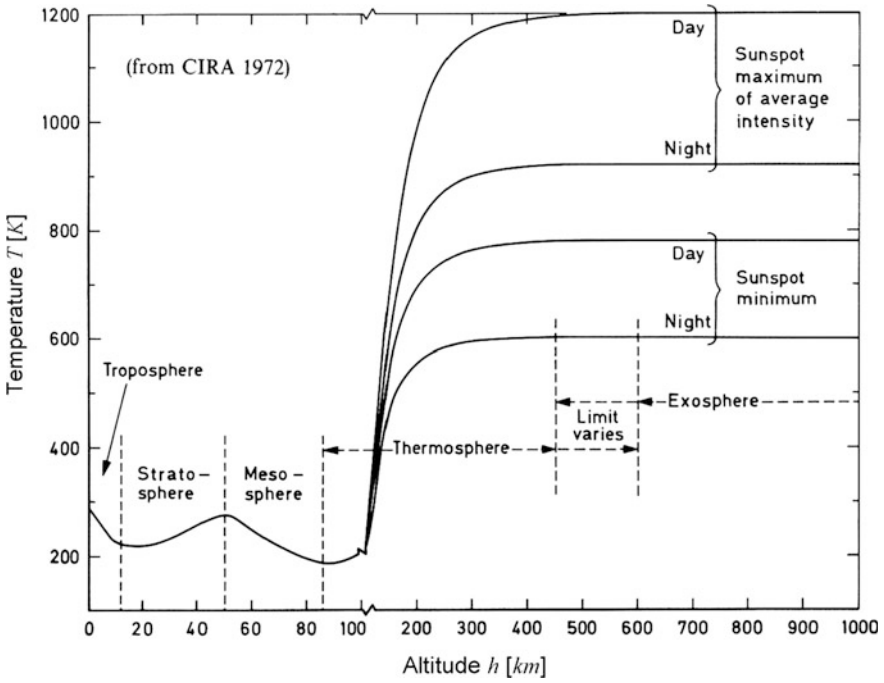

Fig. 6.2 The temperature distribution in Earth's atmosphere. *Credit* King-Hele (1987)

from that in the homosphere in that it displays much higher levels of, and tremendous variations in, temperatures, which are even time-dependent.

The detailed $T(h)$ profile in the homosphere and in the heterosphere is not analytical, so an exact solution to Eq. (6.1.3) can be obtained only by numerical integration. Because this is too intricate for practical applications we have to look for ways to find approximate solutions.

Homosphere (Barometric Formula)

For general purposes the temperature within the homosphere can be considered roughly as constant with a mean value of $T = T_0 \approx 230$ K. For a constant temperature, $dT = 0$, reducing Eq. (6.1.3) to

$$\frac{d\rho}{\rho} = -\frac{R_\oplus^2}{(R_\oplus + h)^2}\frac{dh}{H}$$

Here we have introduced the so-called *scale height* as

$$H := \frac{T_0 R_s}{g_0} = T_0 \cdot 29.28 \left[\text{m K}^{-1}\right] \quad \textbf{scale height}$$

The solution is found by direct integration of both sides yielding

$$\rho = \rho_0 \exp\left[-\frac{R_\oplus h}{(R_\oplus + h)H}\right] \quad @ \quad 0 \le h \le 120 \text{ km} \tag{6.1.4}$$

where h is considered relative to sea level and ρ_0 is the density at sea level. Compared to our assumption $T = const$ we can also safely assume $h \ll R_\oplus$ which leads to the well-known barometric formula

$$\boxed{\rho = \rho_0 \exp\left(-\frac{h}{H}\right)} \quad @ \quad 0 \le h \le 120 \text{ km} \quad \textbf{barometric formula} \tag{6.1.5}$$

If one fits this formula to the actual atmospheric data in the range $0 \le h \le 120$ km one obtains the following mean values for ρ_0, H with errors $\Delta\rho/\rho < 50\%$:

$$\begin{array}{l} \rho_0 = 1.752 \text{ kg m}^{-3} \\ H = 6.7 \text{ km} \end{array} \quad @ \quad 0 \le h \le 120 \text{ km} \tag{6.1.6}$$

Equations (6.1.5) and (6.1.6) are the most convenient and hence the most common form to describe the density distribution in the homosphere. They will be used throughout this book for ascent and reentry of a S/C with sometimes adaptations of the scale height to the actual altitude conditions.

For aerodynamic purposes in later sections we note that in the homosphere of a standard atmosphere with density $\rho(h)$, the Reynolds number of a flight vehicle with speed v is given as

$$Re = 36 \times 10^6 \cdot \exp\left(-\frac{h}{H}\right) \cdot Ma \cdot \frac{l}{L} \propto \rho v$$

with

h altitude
$H = T(h) \cdot 29.28 \left[\text{m K}^{-1}\right] \approx 7.1$ km
Ma Mach number
l characteristic length of the vehicle
$L =$ 1 m.

For a vehicle reentering from space $Re \approx 10^6$.

Heterosphere

Spacecraft orbit Earth at altitudes $h > 100$ km where the atmospheric drag slowly brakes their speed and thus drags them down into lower and lower orbits. To find out their orbit life-times (see Sect. 12.7.4) the detailed density profile at those elevated altitudes needs to be known. Since in the heterosphere temperature varies strongly with height and time and R_s is not constant, a barometric formula like Eq. (6.1.5) does not hold. More appropriate atmospheric models need to be provided which by nature are, however, considerably more complex. Today's quasi-standard is the MSIS-86 model (a.k.a. CIRA-86), which is COSPAR's International Reference Atmosphere, and its newer extension MSIS-E-90. But also

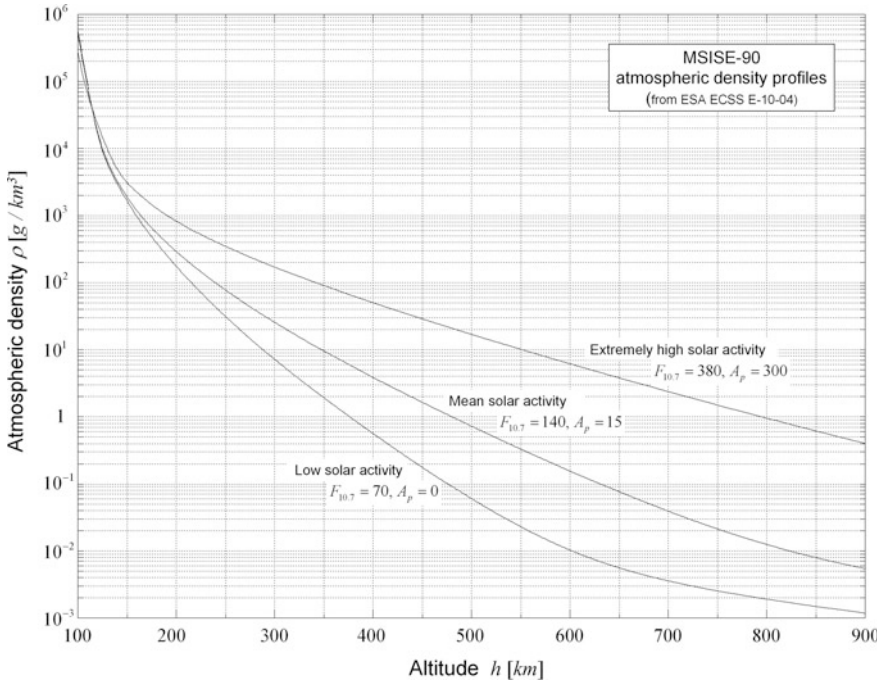

Fig. 6.3 Mean atmospheric density in the heterosphere as derived from the MSIS-E-90 model

the Jacchia 1977 (J77) model and its older variants and the Harris–Priester model from 1962 (see, e.g., Montenbruck and Gill (2000)) are still frequently used. They are all based on piecewise analytical expressions for different altitudes, whose coefficients have been adapted to measured values. So there are no closed analytical expressions and the densities have to be derived numerically. Figure 6.3 depicts the mean atmospheric density profiles as derived from the MSIS-E-90 model above 100 km.

As an illustrative example we present the relatively simple Harris–Priester model. It is based on the data of the upper atmosphere derived from a solution of the heat conduction equation. It takes into account the daily, but not the yearly, temperature variations in the atmosphere. The upper atmosphere expands because of daily insolation and runs about 2 h behind, which corresponds to 30° of longitude toward the east. The density distributions of the corresponding density peaks (maxima, M) and valleys (minima, m) are described by the functions $\rho_M(h)$ and $\rho_m(h)$ by means of piecewise exponential interpolation between interpolation altitudes h_i:

$$\begin{aligned} \rho_m(h) &= \rho_m(h_i)\exp\left(\frac{h_i - h}{H_m}\right) \\ \rho_M(h) &= \rho_M(h_i)\exp\left(\frac{h_i - h}{H_M}\right) \end{aligned} \quad @ \quad h_i < h < h_{i+1} \tag{6.1.7}$$

where h is the altitude above the Earth's reference ellipsoid (see Sect. 12.2.1). The scale heights H_m and H_M are given as

$$H_m(h) = \frac{h_i - h_{i+1}}{\ln \rho_m(h_{i+1})/\ln \rho_m(h_i)}$$
$$H_M(h) = \frac{h_i - h_{i+1}}{\ln \rho_M(h_{i+1})/\ln \rho_M(h_i)}$$

The daily density variation due to insolation is modeled as a cosine variation

$$\rho(h) = \rho_m(h) + [\rho_M(h) - \rho_m(h)] \cdot \cos^n\left(\frac{\Psi}{2}\right)$$

where Ψ is the angle between the position vector of the orbiting S/C and the vector to the density peak. Density variations in geographical latitude are represented by a declinational dependence of Ψ and the exponent n: for a small inclination $n = 2$, and $n = 6$ for polar orbits. Table shows the density coefficients $\rho_M(h)$ and $\rho_m(h)$ at the different interpolation points. Note that above 300 km the atmospheric density differs by a factor of more than two between day-time $\rho_M(h)$ and night-time $\rho_m(h)$ values. This is caused by the large temperature differences in these altitudes between day and night (see Fig. 6.2).

Outer Space

The atmosphere at around 100 km is special in two aspects: First, at this altitude the atmospheric composition changes markedly. Second, above 100 km the heterosphere is so rarefied that it can no longer support aerodynamic flight. To be more specific, the limiting altitude where the flying speed of an airplane would need to reach orbital velocity in order to provide lift that would counteract the gravitational force is called the *Kármán line* and was calculated by Theodore von Kármán to be around 100 km.

For the above two reasons the Fédération Aéronautique Internationale (FAI), which is an international standard setting and record-keeping body for aeronautics and astronautics, defined the border to **outer space** at exactly 100 km. So ***space travelers*** are individuals who have been above 100 km altitude in a vehicle. As opposed to this, in the 1960s the United States adopted the definition of an astronaut as someone having been above at least 50 statute miles (equaling 80 km) altitude. Thus, outer space was and still is indirectly defined by the U.S. as space above 80 km altitude. However, only the FAI's definition is internationally accepted today. It should be noted that from a re-entry point of view the transition from astronautics to aeronautics formally takes place at the so-called entry interface (see Sect. 10.1.2) at 400,000 ft equaling 122 km. In NASA and RKA terms an ***astronaut*** is a crew member of a spacecraft, while other people, who travel aboard spacecraft, are termed ***space flight participants***.

Note that opposed to the above US definition of an astronaut (US astronauts are awarded the *astronaut badge* also called *astronaut wings*) the Association of Space Explorers (ASE, the association of all flown astronauts) defines ***astronauts*** as any "*individuals who have completed at least one orbit of the Earth in a spacecraft*".

Table 6.1 Atmospheric density coefficients of the Harris–Priester model valid for a mean solar activity

h (km)	ρ_m (g km^{-3})	ρ_M (g km^{-3})	h (km)	ρ_m (g km^{-3})	ρ_M (g km^{-3})
100	497400.0	497400.0	420	1.558	5.684
120	24900.0	244900.0	440	1.091	4.355
130	8377.0	8710.0	460	0.7701	3.362
140	3899.0	4059.0	480	0.5474	2.612
150	2122.0	2215.0	500	0.3916	2.042
160	1263.0	1344.0	520	0.2819	1.605
170	800.8	875.8	540	0.2042	1.267
180	528.3	601.0	560	0.1488	1.005
190	361.7	429.7	580	0.1092	0.7997
200	255.7	316.2	600	0.08070	0.6390
210	183.9	239.6	620	0.06012	0.5123
220	134.1	185.3	640	0.04519	0.4121
230	99.49	145.5	660	0.03430	0.3325
240	74.88	115.7	680	0.02632	0.2691
250	57.09	93.08	700	0.02043	0.2185
260	44.03	75.55	720	0.01607	0.1779
270	34.30	61.82	740	0.01281	0.1452
280	26.97	50.95	760	0.01036	0.1190
290	21.39	42.26	780	0.008496	0.09776
300	17.08	35.26	800	0.007069	0.08059
320	10.99	25.11	840	0.004680	0.05741
340	7.214	18.19	880	0.003200	0.04210
360	4.824	13.37	920	0.002210	0.03130
380	3.274	9.955	960	0.001560	0.02360
400	2.249	7.492	1000	0.001150	0.01810

This is why Allan Shepard, the first American in space, internationally is not considered to be America's first astronaut (who is John Glenn) because his space flight in 1961 was just suborbital. Only later Shepard became an astronaut owing to his participation in the Apollo 14 mission. All "Apollo moon flyers" are accepted by ASE as astronauts, because they all have completed at least one Earth orbit before translunar injection. In line with US definition, eight X-15 pilots were awarded astronaut wings in the 1960s because they reached altitudes above 80 km. But only one of them, Joseph A. Walker, flew above 100 km in 1963 (even twice) and therefore is an space traveler by FAI standards, but not an astronaut by ASE standards.

Note that beyond what is referenced here there exists no legal definition of astronaut, neither in the Outer Space Treaties, nor in the International Space Station Legal Framework, nor in the US Commercial Space Launch Act of 1984.

6.1.3 Piecewise-Exponential Model

In later chapters we will study the ascent and reentry of spacecraft through the atmosphere and the orbit life-time of satellites in low Earth orbits. For these studies the barometric formula for the homosphere is too inaccurate, while for the heterosphere the common atmospheric models are too complex to handle analytically. By examining the functional dependency of the atmospheric density in Fig. 6.3 in logarithmic representation, one recognizes that the density can be expressed quite well by piecewise straight lines corresponding to piecewise exponential functions of the form

$$\rho(h) = \rho_i \exp\left(-\frac{h - h_i}{H_i}\right) \quad @ \quad h_i < h < h_{i+1} \tag{6.1.8}$$

where h is the altitude above sea level and h_i are the base altitudes above sea level for a given altitude interval, ρ_i the corresponding nominal base density, and H_i the scale height holding for an entire interval.

They are given for the different altitude intervals in Table 6.2. Equation (6.1.8) is the density model, which we will use in the following for our general analytical studies related to the atmosphere.

Table 6.2 Altitude intervals and corresponding atmospheric coefficients for the piecewise exponential model based on the CIRA-72 atmospheric model

Altitude h (km)	Base altitude h_0 (km)	Nominal density ρ_0 (kg m^{-3})	Scale height H (km)	Altitude h (km)	Base altitude h_0 (km)	Nominal density ρ_0 (kg m^{-3})	Scale height H (km)
0–25	0	1.225	7.249	150–180	150	2.070×10^{-9}	22.523
25–30	25	3.899×10^{-2}	6.349	180–200	180	5.464×10^{-10}	29.740
30–40	30	1.774×10^{-2}	6.682	200–250	200	2.789×10^{-10}	37.105
40–50	40	3.972×10^{-3}	7.554	250–300	250	7.248×10^{-11}	45.546
50–60	50	1.057×10^{-3}	8.382	300–350	300	2.418×10^{-11}	53.628
60–70	60	3.206×10^{-4}	7.714	350–400	350	9.518×10^{-12}	53.298
70–80	70	8.770×10^{-5}	6.549	400–450	400	3.725×10^{-12}	58.515
80–90	80	1.905×10^{-5}	5.799	450–500	450	1.585×10^{-12}	60.828
90–100	90	3.396×10^{-6}	5.382	500–600	500	6.967×10^{-13}	63.822
100–110	100	5.297×10^{-7}	5.877	600–700	600	1.454×10^{-13}	71.835
110–120	110	9.661×10^{-8}	7.263	700–800	700	3.614×10^{-14}	88.667
120–130	120	2.438×10^{-8}	9.473	800–900	800	1.170×10^{-14}	124.64
130–140	130	8.484×10^{-9}	12.636	900–1000	900	5.245×10^{-15}	181.05
140–150	140	3.845×10^{-9}	16.149	1000–	1000	3.019×10^{-15}	268.00

Adopted from Vallado (2007)

6.2 Hypersonic Flow Theory

Imagine a spacecraft that experiences drag in a low Earth orbit or in ascents or reentries through the atmosphere at hypersonic speeds, i.e. at more than about Mach 5. What is the gas flow around the spacecraft and how does it generate the aerodynamic forces on the vehicle? The answer critically depends on whether the atmosphere can be treated as an assembly of free molecules or as an self-interacting gas. Physically we have a gas if the interaction between the molecules is faster than the interaction with the spacecraft. The key parameter is the *mean free path* λ, which is the distance a molecule travels between two successive collisions. The mean free path, of course, depends inversely on the density and hence on the temperature and pressure of the gas $\lambda \propto 1/n \propto T/p$. At sea level the distance between collisions is only $\lambda = 0.066$ μm. At 10 km altitude $\lambda \approx 0.2$ μm, at 50 km $\lambda \approx 80$ μm, at 100 km $\lambda \approx 2$ cm, and 200 km $\lambda \approx 250$ m. For physical effects on the spacecraft the so-called *Knudsen number*, $Kn = \lambda/L$, is relevant, where L is the length scale of the spacecraft. Obviously, if $\lambda \geq L \approx 10$ m, equaling altitudes $h \geq 150$ km, we can treat the atmospheric gas as an assembly of individual non-interacting molecules and hence $Kn \geq 1$. This is called *free molecular flow regime*. For $Kn < 0.03$, i.e. at altitudes $h \leq 90$ km, the atmosphere can be modelled as a continuum, and for $0.03 < Kn < 1$, i.e. 90 km $< h <$ 150 km, we are in a *transition regime*. Since a spacecraft upon ascent or reentry passes all three regimes we need to study them all.

Free molecular flow regime	$Kn \geq 1$	$h \geq 150$ km
Transition regime	$0.03 < Kn < 1$	90 km $< h <$ 150 km
Continuum regime	$Kn < 0.03$	$h \leq 90$ km

In the following general study of the aerodynamic forces of a vehicle, namely lift and drag, let ρ be the atmospheric mass density at a given altitude, m the mass of the vehicle, $A_\perp$ its cross-sectional area (wetted surface area) with regard to the flight direction, and v its velocity relative to the atmosphere, which to a high accuracy is identical to the speed of the S/C measured relative to the ground.

6.2.1 Free Molecular Flow

We first study the effects of free molecular flow, valid for $Kn \geq 1$ equaling altitudes $h \geq 150$ km. In this case we can treat the gas as an assembly of non-interacting molecules that behave fully ballistically. We therefore can apply statistical mechanics, from which the aerodynamic forces are simply determined by the linear

momentum transfer of the atmospheric particles per unit time. In the scattering process we define

Δp as the momentum transfer to the surface,

$\Delta p_{||}$ the proportion of momentum that is transferred in the flow direction $\hat{\boldsymbol{p}}$, *and*

$\Delta p_{\perp}$ the portion that is transferred into the direction $\hat{\boldsymbol{p}}_{\perp}$, lying in the reflection plane normal to $\hat{\boldsymbol{p}}$, i.e., $\hat{\boldsymbol{p}}\,\hat{\boldsymbol{p}}_{\perp} = 0$

All these momentum transfers critically depend on the details of the ballistic reflection process from the surface. Quite formally, if an impacting particle initially possess linear momentum p, the amount of momentum that is transferred to the surface depends on one hand on the incidence angle θ measured relative to the surface normal, and on the other hand on the way the particle is scattered off the surface and hence on the details of the scattering process (denoted by the symbol $\times$), which depends for instance on the surface (e.g., surface roughness) and boundary layer properties. These scattering details are comprised by the dimensionless momentum transfer functions $f_{||,\times}(\theta)$ and $f_{\perp,\times}(\theta)$ defined by

$$\begin{aligned} p \cdot f_{||,\times}(\theta) &:= \Delta p_{||} = \Delta \boldsymbol{p} \cdot \hat{\boldsymbol{p}} \\ p \cdot f_{\perp,\times}(\theta) &:= \Delta p_{\perp} = \Delta \boldsymbol{p} \cdot \hat{\boldsymbol{p}}_{\perp} \end{aligned} \tag{6.2.1}$$

$f_{||,\times}(\theta)$ and $f_{\perp,\times}(\theta)$ are known theoretically only for some elementary surface shapes (see e.g. Sect. 6.2.4). So, in general they are determined experimentally.

Based on the moment transfer, the aerodynamic drag and lift (which are the absolute values of the corresponding force vectors) on $A_{\perp}$ are given by Newton's second law (see Eq. 7.1.12 and Remark thereafter) as

$$\begin{aligned} D &= \frac{d\left(\Delta p_{||}\right)}{dt} = f_{||,\times}\frac{dp}{dt} = f_{||,\times}\frac{d(mv)}{dt} = f_{||,\times} v\,\dot{m} = f_{||,\times}\rho v^2 A_{\perp} \\ L &= \frac{d(\Delta p_{\perp})}{dt} = f_{||,\times}\frac{dp}{dt} = f_{\perp,\times}\frac{d(mv)}{dt} = f_{\perp,\times} v\,\dot{m} = f_{\perp,\times}\rho v^2 A_{\perp} \end{aligned}$$

where the latter follows from the continuity equation (see Eq. (1.2.8)) of the air flow, $\dot{m} = \rho v A_{\perp}$. From this derivation we recognize that the quadratic velocity dependence on one hand is due to the momentum transfer and on the other to the number of particles hitting the surface per unit time, both of which are proportional to the impinging velocity. To calculate the aerodynamic drag and lift of the entire S/C, the drag and lift of an infinitesimal surface area $dA_{\perp}$

$$\begin{aligned} dD &= f_{||,\times}\rho v^2 \cdot dA_{\perp} = f_{||,\times}\cos\theta \cdot \rho v^2 \cdot dA \\ dL &= f_{\perp,\times}\rho v^2 \cdot dA_{\perp} = f_{\perp,\times}\cos\theta \cdot \rho v^2 \cdot dA \end{aligned}$$

with different θ and/or surface properties have to be integrated over the total wetted area

$$D = \rho v^2 \iint_A f_{\parallel,\times}(\theta) \cos\theta \cdot dA \tag{6.2.2a}$$

$$L = \rho v^2 \iint_A f_{\perp,\times}(\theta) \cos\theta \cdot dA \tag{6.2.2b}$$

Specular and Diffuse Reflection

For specular and diffuse reflection the momentum transfer functions can easily be evaluated. From Fig. 6.4 we deduce that for specular reflection the momentum transfer to the surface is

$$\Delta \boldsymbol{p} = -2p \cos\theta \cdot \boldsymbol{n} \quad @ \quad \text{specular reflection} \tag{6.2.3}$$

where

$$\boldsymbol{n} = -(\cos\theta\, \hat{\boldsymbol{p}} + \sin\theta\, \hat{\boldsymbol{p}}_\perp)$$

is the surface normal vector. For diffuse reflection we must average the momentum transfer over all reflection angles. One generally assumes that the reflected intensity is proportional to the angle of the reflected molecule from $\boldsymbol{n}$. This leads to

$$\Delta \boldsymbol{p} = -p \cos\theta \cdot \left(\frac{2}{3}\boldsymbol{n} - \hat{\boldsymbol{p}}\right) \quad @ \quad \text{diffuse reflection} \tag{6.2.4}$$

Applying these results to Eqs. (6.2.1) we find the longitudinal and transverse transfer functions

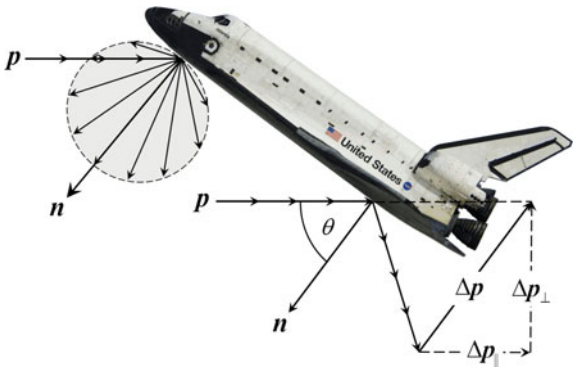

Fig. 6.4 Schematics of diffuse (top) and specular (bottom) reflection

$$\begin{aligned} f_{||,\,spec} &= 2\cos^2\theta \\ f_{\perp,\,spec} &= 2\sin\theta\,\cos\theta \end{aligned} \quad @\ \text{specular reflection} \tag{6.2.5}$$

and

$$\begin{aligned} f_{||,\,diff} &= \cos\theta\left(\tfrac{2}{3}\cos\theta + 1\right) \\ f_{\perp,\,diff} &= \tfrac{2}{3}\sin\theta\,\cos\theta \end{aligned} \quad @\ \text{diffuse reflection} \tag{6.2.6}$$

For the specular and diffuse drag and lift we therefore obtain with Eqs. (6.2.2a) and (6.2.2b) for a flat plate with surface A and hence wetted area $A_\perp = A\,\cos\theta$

$$\begin{aligned} D_{spec} &= 2\rho v^2 A\,\cos^3\theta \\ L_{spec} &= 2\rho v^2 A\,\sin\theta\,\cos^2\theta \end{aligned} \quad @\ \text{flat plate specular reflection} \tag{6.2.7}$$

and

$$\begin{aligned} D_{diff} &= \rho v^2 A\,\cos^2\theta\left(\tfrac{2}{3}\cos\theta + 1\right) \\ L_{diff} &= \tfrac{2}{3}\rho v^2 A\,\sin\theta\,\cos^2\theta \end{aligned} \quad @\ \text{flat plate diffuse reflection} \tag{6.2.8}$$

Assuming only specular reflection from a flat plate we find for the so-called lift-to-drag ratio

$$\frac{L_{spec}}{D_{spec}} = \tan\theta \tag{6.2.9}$$

This is a celebrated result because it generally holds for the three regimes: inviscid supersonic, hypersonic, and free molecular flow over a flat plate.

Depending on the surface roughness one has a mix of specular and diffuse scattering for a concrete S/C surface in the free molecular flow regime.

6.2.2 *Newtonian Flow Theory*

We now turn to the hypersonic flow for $Kn < 1$, i.e. in the continuum regime with $Kn < 0.03$ and, at lower altitudes, in the transition regime with $0.03 < Kn < 1$. Here scattering between the gas molecules and hence gas dynamics needs to be accounted for.

A key feature of hypersonic flow is that the Mach angle is so small that the incoming stream lines are deflected nearly parallel and close to the surface making up a thin shock layer, as depicted in Fig. 6.5. Consequently,

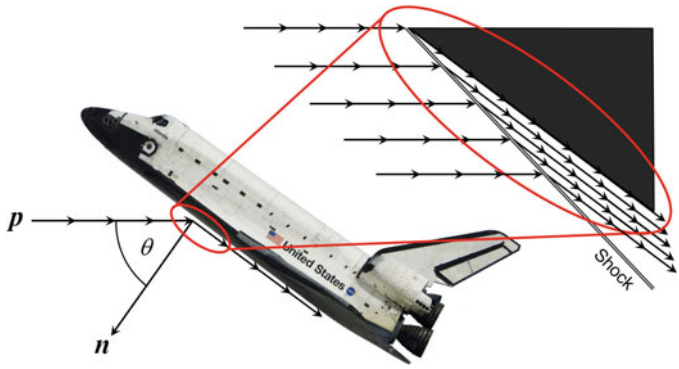

Fig. 6.5 Streamlines of hypersonic flow in Newtonian flow theory

1. the flow around a hypersonic body and the corresponding aerodynamics loses importance
2. the strong interaction, i.e. friction, between the surface layer and the body surface causes extreme gas temperatures leading to molecular vibrations and even dissociation, which causes alterations from the ideal gas concept.

Because this behavior resembles Newton's gas flow theory that he established at the end of the 17th century for wind flow around buildings, the corresponding flow theory is frequently called Newtonian flow theory, or Newtonian theory for short.

Gas Dynamics at Hypersonic Speeds

While for the main atmospheric components dissociation $O_2 \rightarrow O + O$ and $N_2 \rightarrow N + N$ commences at $v \geq 2\,\mathrm{km/s}$ and $v \geq 5\,\mathrm{km/s}$, they ionize only at $v \geq 11\,\mathrm{km/s}$. Therefore, in the case when a spacecraft such as a Space Shuttle or capsule reentries from Earth orbits with $v \approx 7.9\,\mathrm{km/s}$, ionization effects only occur partitially at stagnation points and hence are negligible, while dissociation effects in principle are relevant. Yet, dissociation has only a very mild, (and hence for our considerations also negligible), effect on lift and drag.

> **Remark** *For the Shuttle, dissociation varied considerably along the centerline and thus had a considerable effect on the pitching moment of the Shuttle. To be specific, due to these chemical effects the body flap deflection for pitch trim turned out to be twice as big as initially predicted and designed for the Shuttle. Therefore, for all Shuttle reentries body flap deflection was always at its limit and therefore under NASA's close observation.*

Therefore, we limit our analysis to ideal gas dynamics. This essentially implies that we will not consider chemical effects such as dissociation or ionization of atmospheric components at hypersonic velocities.

Hypersonic Flow Dynamics

We do not want to go into the details of hypersonic flow dynamics. For this we refer to classical textbooks (see e.g. Anderson (2006)) and summarize here only those results, which are significant to determine the aerodynamic forces on a hypersonic vehicle.

As stated above the characteristics of hypersonic flow is that after impact the stream lines are nearly parallel to the surface. In microscopic terms this means that the molecules lose their momentum normal to the surface but preserve their tangential momentum as shown in Fig. 6.5. In effect, we have the following momentum transfer laws (cf. Eq. (6.2.3))

$$\Delta \boldsymbol{p} = p \cos\theta \cdot \boldsymbol{n} \tag{6.2.10}$$

which due to $f_{\|,\times} \propto \Delta\hat{\boldsymbol{p}} \cdot \hat{\boldsymbol{p}}$, $f_{\perp,\times} \propto \Delta\hat{\boldsymbol{p}} \cdot \hat{\boldsymbol{p}}_{\perp}$ leads to

$$\begin{aligned} f_{\|,sld} &= \cos^2\theta \\ f_{\perp,sld} &= \sin\theta\cos\theta \end{aligned} \quad @ \text{ surface layer deflection} \tag{6.2.11}$$

that is, their values are only half of that in the free flow regime. Accordingly

> Although for hypersonic flow the values of the drag and lift coefficients, and hence also for drag and lift, attain only half of the values for free molecular flow, the $L/D = \tan\theta$ law holds in both flow regimes.

Since this results applies to any infinitesimally small flat surface it holds for any body shape.

Skin Friction Drag

However, apart from a modified scattering process the shear forces of the skin flow exert the following skin friction drag on the reentry vehicle surface

$$D_f = \frac{1}{2}\rho v^2 C_f A \tag{6.2.12}$$

Here C_f is the *skin friction drag coefficient*, which for turbulent boundary flow depends only weakly on the Reynolds number in the following way

$$C_f = 0.074 \cdot \mathrm{Re}^{-1/5} = C_{f0}\left(\frac{\rho_0 v_0}{\rho v}\right)^{1/5} \quad \begin{matrix}\textbf{skin friction} \\ \textbf{drag coefficient}\end{matrix} \tag{6.2.13}$$

$$\rho_0 v_0 = 1.2041 \ \ \mathrm{kg\ m^{-3}} Ma$$

where ρv is the mass flux on the surface and C_{f0} the skin friction drag coefficient, both at standard atmosphere and $Ma = 1$.

Transition regime
In the transition regime gas dynamics changes from non-slip to slip conditions and thus gas pressure changes in the boundary layer. Nevertheless, the *L/D* ratio, which was derived simply from geometrical considerations, remains unaffected. We therefore are saved from extending the result $L/D = \tan\theta$ of the Newtonian limit into the transition regime as long as the gas interaction is sufficient to create a boundary layer with a gas pressure.

6.2.3 Drag and Lift Coefficients

Owing to the specific microscopic unevenness of actual S/C surfaces (surface roughness) drag and lift obviously cannot be evaluated analytically, and often not even numerically from the integrals Eqs. (6.2.2a) and (6.2.2b). One therefore and even quite generally resorts to defining a dimensionless "effective force conversion coefficient"

$$C := \frac{\text{force}}{(\text{dynamic pressure}) \times A_\perp} \tag{6.2.14}$$

where the dynamic (air) pressure is defined as $p_a := \frac{1}{2}\rho v^2$. Observe that through *Bernoulli's principle* $p_a A_\perp = \frac{1}{2}\rho v^2 A_\perp \propto \frac{1}{2}mv^2 = E_{kin}$ the denominator is closely related to the kinetic energy of the impacting particles. With the above definition we obtain from Eq. (6.2.2a)

$$D = \frac{1}{2}\rho v^2 C_D A_\perp \tag{6.2.15a}$$

with the "effective along-force conversion coefficient", better known as the *drag coefficient,*

$$C_D = \frac{2}{A_\perp}\iint_{A_\perp} f_{\|,\times}(\theta)\cdot dA_\perp = \frac{2}{A_\perp}\iint_{A} f_{\|,\times}(\theta)\cos\theta\cdot dA \quad \textbf{drag coefficient} \tag{6.2.15b}$$

Owing to the normalization to $A_\perp$, this dimensionless drag coefficient only depends on the shape of the body (and not on its size) and on the detailed interaction of the impacting particles with the surface. By the same token, the lateral lift can be determined from Eq. (6.2.2b) as

$$L = \frac{1}{2}\rho v^2 C_L A_\perp \tag{6.2.16a}$$

with the dimensionless lift coefficient

$$C_L = \frac{2}{A_\perp} \iint\limits_{A_\perp} f_{\perp,\times}(\theta) \cdot dA_\perp = \frac{2}{A_\perp} \iint\limits_{A} f_{\perp,\times}(\theta) \cos\theta \cdot dA \quad \textbf{lift coefficient} \tag{6.2.16b}$$

Note *Note that the seemingly odd factor 2 is well-established by reference to the kinetic energy of the impacting particles. Despite this, the use of a drag coefficient defined without the factor 2 is not uncommon in the literature. Therefore, caution is always in order.*

Reduced Coefficients
For later practical purposes we also define the *reduced drag coefficient* and *reduced lift coefficient*

$$\kappa_D := \frac{C_D}{2} \frac{A_\perp H}{m} \rho_0 = \frac{1}{2} \rho_0 BH \quad \textbf{reduced drag coefficient} \tag{6.2.17}$$

$$\kappa_L := \frac{C_L}{2} \frac{A_\perp H}{m} \rho_0 = \kappa_D \frac{C_L}{C_D} = \kappa_D \frac{L}{D} \quad \textbf{reduced lift coefficient} \tag{6.2.18}$$

For hypersonic speeds we typically have $\kappa_D \approx 25$.

Ballistic Coefficient
Besides drag and lift coefficients another frequently used characteristic parameter of a S/C with mass m is

$$B := C_D \frac{A_\perp}{m} \quad \textbf{ballistic coefficient} \tag{6.2.19}$$

Consider the ballistic coefficient as a single characteristic aerodynamic parameter where all the unknowns of a S/C are lumped together. It can best be determined experimentally from the decay data of a S/C's low Earth orbit as provided by NORAD TLE and from Eq. (12.7.20) in Sect. 12.7.4. Note that in literature the ballistic coefficient is often defined inversely, i.e., $B = m/(C_D A_\perp)$, which can be recognized by its inverse dimensions.

6.2.4 Drag in Free Molecular Flow

In this section we consider simple specific geometric bodies in free molecular flow. The geometries are assumed to be either symmetric relating to the flight direction or that the bodies are tumbling so that their average shape is symmetric. In both cases the bodies do not experience any lift. We therefore study now only their drag coefficients.

Cone

We start with a cone having an aperture angle 2α. If its symmetry axis points along the direction of motion, any gas molecule strikes the surface at the same angle $\theta = 90° - \alpha$ and therefore we have according to Eqs. (6.2.5) and (6.2.6)

$$C_{D,spec} = 2f_{||,\,spec} = 4\sin^2\alpha \leq 4$$
$$C_{D,diff} = 2f_{||,\,diff} = 2\sin\alpha\left(\frac{2}{3}\sin\alpha + 1\right) \leq 3.333$$

Thus, a cone aerodynamically behaves like a plate with its drag depending only on its slenderness. The more slender the cone the less its drag. From these results we derive the following relationships for specular and diffuse drag of a cone

$$C_{D,spec} = C_{D,diff} = 2.25 \quad @ \quad \alpha = \arcsin 3/4 = 48.6°$$
$$C_{D,spec} \geq C_{D,diff} \quad @ \quad \alpha \geq 48.6°$$

Sphere

For a sphere we find for the drag coefficients evaluated over a wetted half sphere

$$C_{D,spec} = \frac{2}{A_\perp}\frac{A}{2\pi}\int_{2\pi} f_{||,spec}(\theta)\cos\theta \cdot d\Omega = \frac{2}{\pi r^2}\frac{2\pi r^2}{2\pi}\int_0^{2\pi}\int_0^{\pi/2} 2\cos^3\theta \cdot \sin\theta \cdot d\theta \cdot d\varphi$$
$$= 8\int_0^{\pi/2}\cos^3\theta\,\sin\theta \cdot d\theta = 8\left(-\frac{1}{4}\cos^3\theta\right)\Big|_0^{\pi/2} = 2$$

$$C_{D,diff} = \frac{2}{A_\perp}\frac{A}{2\pi}\int_{2\pi} f_{||,diff}(\theta)\cos\theta \cdot d\Omega = \frac{2}{\pi r^2}\frac{2\pi r^2}{2\pi}\int_0^{2\pi}\int_0^{\pi/2}\cos^2\theta\left(\frac{2}{3}\cos\theta + 1\right)\cdot\sin\theta \cdot d\theta \cdot d\varphi$$
$$= 4\int_0^{\pi/2}\left(\frac{2}{3}\cos^3\theta\sin\theta + \cos^2\theta\sin\theta\right)\cdot d\theta = 4\left(-\frac{2}{12}\cos^4\theta - \frac{1}{3}\cos^3\theta\right)\Big|_0^{\pi/2} = 2$$

Tumbling Cuboid

We finally assume a tumbling cuboid, which might come closest to the shape of a general satellite. We define our Cartesian reference frame such that the x-axis points along the flight direction of the body and the y- and z-axes normal to it. Accordingly, the surface areas of the cuboid with normal vectors pointing in the three axis directions are termed A_x, A_y, A_z. We introduce standard spherical coordinates with the polar angle θ relative to the z-axes and the azimuthal angle φ relative to the x-axes. We thus have for the three wetted areas

$$\begin{aligned} A_{\perp x} &= A_x \cos\varphi \, \sin\theta \\ A_{\perp y} &= A_y \sin\varphi \, \sin\theta \\ A_{\perp z} &= A_z \cos\theta \end{aligned} \tag{6.2.20}$$

To simplify calculations we make the assumption that the cuboid tumbles along a rotational axis, which is lateral to the direction of motion, i.e. $\varphi = 0$. In this case $A_{\perp x} = A_x \sin\theta$, $A_{\perp y} = 0$, $A_{\perp z} = A_z \cos\theta$ and we have to average the following expressions

$$C_{D,spec} = 2\frac{2\cos^2(90^\circ - \theta)\cdot A_{\perp x} + 2\cos^2\theta \cdot A_{\perp z}}{A_{\perp x} + A_{\perp z}} = 4\frac{\cos^3\theta + \lambda \, \sin^3\theta}{\cos\theta + \lambda \, \sin\theta}$$

$$\begin{aligned} C_{D,diff} &= 2\frac{\left[\cos\theta\left(\frac{2}{3}\cos\theta + 1\right)\right]\cdot A_z\cos\theta + \left[\sin\theta\left(\frac{2}{3}\sin\theta + 1\right)\right]\cdot A_x\sin\theta}{A_z\cos\theta + A_x\sin\theta} \\ &= 2\left[\frac{2}{3}\frac{\cos^3\theta + \lambda \, \sin^3\theta}{\cos\theta + \lambda \, \sin\theta} + \frac{\cos^2\theta + \lambda \, \sin^2\theta}{\cos\theta + \lambda \, \sin\theta}\right] \end{aligned}$$

where

$$\lambda := \frac{A_x}{A_z}$$

over a quarter rotation. With the use of a symbolic integrator we find

$$\left\langle \frac{\cos^3\theta + \lambda \, \sin^3\theta}{\cos\theta + \lambda \, \sin\theta} \right\rangle_\theta = \frac{2}{\pi\left(1+\lambda^2\right)}\left[\pi\left\{\frac{1}{4}\left(1+\lambda^2\right) + \frac{\lambda^2}{1+\lambda^2}\right\} - \lambda - \lambda\frac{1-\lambda^2}{1+\lambda^2}\ln\lambda\right]$$

$$\left\langle \frac{\cos^2\theta + \lambda \, \sin^2\theta}{\cos\theta + \lambda \, \sin\theta} \right\rangle_\theta = \frac{2}{\pi\left(1+\lambda^2\right)}\left[(1-\lambda)^2 + 2\frac{\lambda(1+\lambda)}{\sqrt{1+\lambda^2}}\cdot \operatorname{artanh}\left(\frac{\sqrt{1+\lambda^2}}{1+\lambda}\right)\right]$$

For $0 \le \lambda \le 1$ both functions are strictly monotonically increasing and vary by less than 18% from an mean value at $\lambda = 0.1$.

Tumbling Cube

To arrive at concrete numbers we now assume that we have a cube, $A \equiv A_x = A_y = A_z$, i.e. $\lambda = 1$. In this case we find

$$\left\langle C_{D,spec}\right\rangle_\theta = 4\left(1 - \frac{1}{\pi}\right) = 2.73 \quad @ \text{ tumbling cube}$$

and

$$\left\langle C_{D,diff}\right\rangle_\theta = 2\left[\frac{2}{3}\left(1 - \frac{1}{\pi}\right) + \frac{2\sqrt{2}}{\pi}\cdot \operatorname{artanh}\left(\frac{1}{\sqrt{2}}\right)\right] = 2.50 \quad @ \text{ tumbling cube}$$

So, the average drag owing to diffuse reflection is little less than that owing to specular reflection.

Standard Drag and Lift Coefficient Approximation
In conclusion of these examples we can state that

> For a body with arbitrary shape in free molecular flow the specular and diffuse reflection for both lift and drag is about the same; the drag coefficient amounts to about little more than 2.0 (sphere). For tumbling or irregular shapes the lift coefficient vanishes.

In face of the fact that the surfaces of spacecraft are highly irregular and therefore the drag coefficient generally is only roughly known, it is not worth discerning these two types of reflections in the free molecular flow regime. We will therefore consider only single average drag and single average lift coefficients

$$\begin{aligned} C_D &\equiv \langle C_D \rangle = \langle C_{D,spec} \rangle \approx \langle C_{D,diff} \rangle \\ C_L &\equiv \langle C_L \rangle = \langle C_{L,spec} \rangle \approx \langle C_{L,diff} \rangle \end{aligned} \tag{6.2.21}$$

for further analysis.

As a matter of fact, the more irregular the shape of a body is and if we go from 2-dimensional to 3-dimensional shapes and averages for tumbling bodies, the better the following empirical and frequently used rough value for the drag coefficient becomes

$$\boxed{C_D = 2.2 \pm 0.2} \quad @\ 150\ \text{km} < h < 600\ \text{km} \tag{6.2.22}$$

This value is comprehensible because it falls between the value for the shape of a sphere and a tumbling cube (see results above). For a laterally tumbling cuboid $C_D \approx \left(\langle C_{D,spec} \rangle + \langle C_{D,diff} \rangle\right)/2 = 2.2$ holds if $A_z/A_x = \lambda = 0.046$.

The above empirical value is quite crude. Actually, the drag coefficient depends on the chemical composition of the atmosphere, because both the energy transfer and the molecular speed ratio decrease as the molecular weight of the atmosphere decreases with changing molecular constituents of the atmosphere. The drag coefficient with respect to atomic oxygen (prevailing at 200–600 km altitude) is approximately 2.2, while with respect to helium (prevailing at 600–1500 km) it approximates 2.8. However, when solar activity becomes low (F10.7 < 80), helium becomes dominant at altitudes as low as 500 km. Above 1500 km, when hydrogen becomes the dominant species, the drag coefficient value is greater than 4.0. This matches the reported drag coefficient for spheres, which increases slightly from 2.2 at 250 km to 2.4 at 500 km altitude. Therefore, the drag coefficient and with it the ballistic coefficient (see below) can vary by as much as 80% over a wide range of altitudes.

Geometric Bodies in Newtonian Flow
We have seen in Sect. 6.2.2. that for Newtonian flow the drag and lift coefficient attain values only half of those for free molecular flow. Therefore the above results

also apply to Newtonian flow if the obtained results are divided by 2. More generally it can be said that

> In free molecular flow the values of drag and lift coefficients are of order 2, while in Newtonian flow they are of order 1.

6.2.5 Aerodynamic Forces

With all these definitions the drag in Eq. (6.2.15a) can be written with the barometric formula Eq. (6.1.5) as

$$D = \frac{1}{2}\rho v^2 C_D A_\perp = m v^2 \frac{\kappa_D}{H} \mathrm{e}^{-\frac{h}{H}} = \frac{1}{2} m B \rho v^2 \quad \textbf{drag} \tag{6.2.23}$$

Example

What is the mean atmospheric drag of the International Space Station ($h = 350$ km, $m = 419$ t, $A_\perp \approx 1050\ \mathrm{m}^2$, $C_D \approx 2.2$)?

The ballistic coefficient according to Eq. (6.2.19) is $B \approx 0.0055\ \mathrm{m}^2\,\mathrm{kg}^{-1}$. At an altitude of 350 km the average atmospheric mass density is $\langle\rho\rangle = 9.518\ \mathrm{g\,km}^{-3}$. With this we calculate the drag and the deceleration to be $a_D = D/m = 1.5 \times 10^{-6}\ \mathrm{m\,s}^{-2} = 0.15\ \mu g_0$, where $g_0 = 9.798\ \mathrm{m\,s}^{-2}$ is Earth's mean gravitational acceleration at its surface.

Remark *This residual atmospheric acceleration force is not the primary contribution to the so-called* µg condition *onboard the scientific laboratories of the ISS. By far the biggest share is the tidal forces (see Sect. 8.5.2) with $a \approx 1\ \mu g_0$ per meter distance from the center of mass of the ISS. This is where the expression "microgravity research" for scientific research in space comes from.*

Of course the drag force always points antiparallel to the velocity vector $\boldsymbol{D} = -D\hat{\boldsymbol{v}} = -D\boldsymbol{u}_t$ (see Figs. 6.6 and 6.7).

Remark *In line with the literature we discriminate between the notation "drag/lift" and "drag/lift forces". A drag/lift force is the force vector caused by the interaction of the air flow with the vehicle, while drag/lift is the amount of this vector.*

On the other hand and according to the definition, the lift vector $\boldsymbol{L} \perp \boldsymbol{D}$. This leaves a degree of freedom for $\boldsymbol{L}$ in the plane vertical to the flight direction (see Fig. 6.7). As S/C in low Earth orbits or at hypervelocity speeds are moving in a plane (see Sects. 6.3 and 7.2.2), usually only the in-plane component of the lift is relevant (see Fig. 6.7). In line with the literature we therefore define $L_v := \boldsymbol{L}\boldsymbol{u}_n$, i.e., L is the "outward"-component of $\boldsymbol{L}$ in the plane. Because the plane usually includes Earth's center of mass, this lift component is also known as (upward) vertical lift. This implies

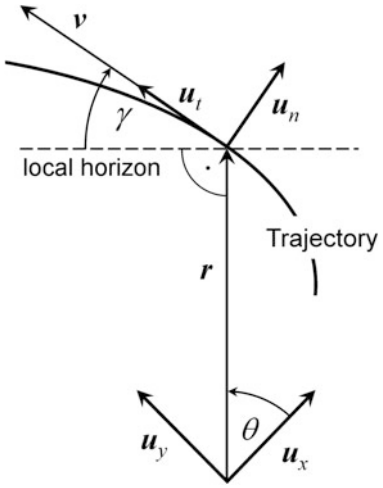

Fig. 6.6 The co-moving S/C reference system $(\boldsymbol{u}_t, \boldsymbol{u}_n)$ and the inertial Earth reference system $(\boldsymbol{u}_x, \boldsymbol{u}_y)$

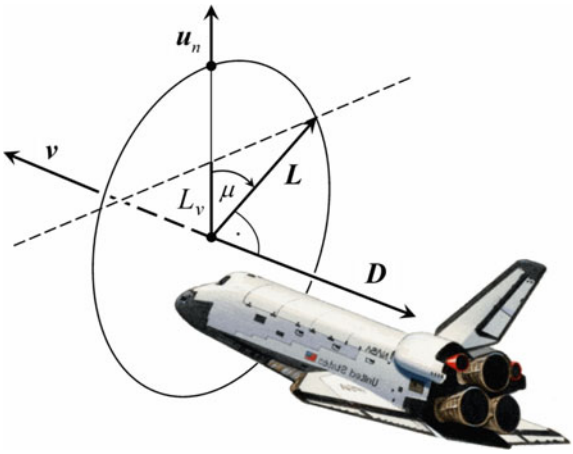

Fig. 6.7 The orientation of drag and lift forces in the co-moving S/C system

that L_v actually depends on the orientation of $\boldsymbol{L}$ as given by the so-called **bank angle** μ. The lift therefore is written as

$$L = \frac{1}{2}\rho v^2 C_L A_\perp = mv^2 \frac{\kappa_L}{H} e^{-\frac{h}{H}} \quad \textbf{lift} \tag{6.2.24}$$

and

$$L_v = L\cos\mu \quad \textbf{vertical lift}$$
$$L_h = L\sin\mu \quad \textbf{horizontal lift}$$

By turning $\boldsymbol{L}$ sideways the horizontal lift provides a cross-range capability of the space vehicle (see, e.g., Space Shuttle reentry, Sect. 10.7.1). By turning the vehicle

down, $\mu = 180°$, one can even achieve a negative vertical lift, $L_v < 0$, as utilized, for instance, for Apollo reentries (see Sect. 10.5.2).

***L/D* Ratio**

From Eqs. (6.2.23) and (6.2.24) we find for the lift-to-drag ratio, L/D, which is a key parameter for reentry flight mechanics (see Sect. 10.2.1),

$$\frac{L}{D} = \frac{C_L}{C_D} \tag{6.2.25}$$

L/D actually is not constant, but largely depends on the angle of attack (AOA) α, which is the angle between the body's reference line and the oncoming flow, and somewhat also on the atmospheric density and relative speed. For hypersonic speeds, we typically have $L/D = C_L/C_D = 0.2 - 2.5$.

The lesser values apply for capsule-shaped blunt bodies. For the Apollo 4 capsule reentry the following measured relation was found in the transition and continuum regime

$$\frac{L}{D} = 0.0143 \cdot \alpha\,[°] \quad @\ \text{Apollo capsule}, \alpha = 0° - 40° \tag{6.2.26}$$

Here α is the angle in units of degrees between the flight vector and the body center line in flight direction. On average $C_D \approx 1.22$, $C_L \approx 0.45$, $L/D = 0.369$ was measured during entry.

For winged bodies, such as the Space Shuttle, the wings and the body as a rough approximation, constitute a flat plate for the hypervelocity flow. So, the angle of attack α is related to the air flow incidence angle θ through $\theta = 90° - \alpha$. Assuming that specular and diffuse scattering are about the same (see Eq. (6.2.21)), we derive from Newtonian flow theory in the continuum regime, i.e. Eq. (6.2.11) inserted into Eqs. (6.2.2a) and (6.2.2b) and with Eqs. (6.2.12) and (6.2.13)

$$\begin{aligned} D &= \rho v^2 A \sin^3\alpha + \frac{1}{2}\rho v^2 C_f A \\ L &= \rho v^2 A \sin^2\alpha \cos\alpha \end{aligned} \tag{6.2.27}$$

The drag on the spacecraft therefore monotonically increases with AOA and becomes maximal for $\alpha = 90°$. Lift also increases with increasing AOA, but becomes maximal for $\alpha = 65.5°$, and decreases thereafter. This is what one intuitively expects and what resembles the general behavior of a spacecraft at hypersonic speeds. So, in general the expression

$$\frac{L}{D} = \frac{\sin\alpha \sin 2\alpha}{2\sin^3\alpha + C_f} \quad @\ \text{winged body}, v \geq 5\ Ma \tag{6.2.28}$$

$$C_f = C_{f0}\left(\frac{\rho_0 v_0}{\rho v}\right)^{1/5}, \quad \rho_0 v_0 = 1.2041 \ \text{kg m}^{-3} Ma$$

describes the AOA-dependent lift-to-drag ratio of a hypervelocity vehicle quite well. Observe that owing to the skin friction L/D does not diverge at $\alpha = 0$, but displays a maximum of $L/D_{\max} = 1 - 2.5$ at typically $\alpha \approx 20°$. From extensive trajectory data of the first Space Shuttle mission STS-1 it can be derived that

$$C_{f0} = 0.0210 \pm 0.0005 \quad @ \ \text{Space Shuttle}, v \geq 3 \ Ma \tag{6.2.29}$$

6.3 Equations of Motion

It is our goal to derive the equations of motion of a S/C flight in the atmosphere of a celestial body. We start out with the general equation of rocket motion (1.1.7)

$$m\dot{\boldsymbol{v}} = \boldsymbol{F}_* + \boldsymbol{F}_{ext}$$

where $\boldsymbol{F}_* = \dot{m}\boldsymbol{v}_*$ is the thrust of the rocket, and $\boldsymbol{F}_{ext}$ comprises all external forces, in particular the aerodynamic forces, which are distinctive for this situation. Figure 6.8 shows the flight path of a rocket in the atmosphere with flight direction $\boldsymbol{v}$ and all relevant forces at a given point in flight. Given these forces, the equation of motion can be explicitly written as

$$m\frac{d\ddot{\boldsymbol{r}}}{dt} = \boldsymbol{F}_*(t) + m\boldsymbol{g}(\boldsymbol{r}) + \boldsymbol{D}(\boldsymbol{v}, \boldsymbol{r}) + \boldsymbol{L}(\boldsymbol{v}, \boldsymbol{r}) \tag{6.3.1}$$

For a given S/C the altitude- and velocity-dependent drag $\boldsymbol{D}$, lift $\boldsymbol{L}$, and the time-dependent thrust $\boldsymbol{F}_*$ is known, and they can be used to solve Eq. (6.3.1) numerically. The solution is the wanted $\boldsymbol{r}(t)$ and $\boldsymbol{v}(t) = d\boldsymbol{r}/dt$. For real missions, this indeed is the only possibility to determine the solution with adequate accuracy.

This would already bring us to the end of this chapter, were it not for the need to gain a physical understanding of the processes and typical flight stages. For that we first introduce appropriate reference systems, which is always an essential step when exploring physical processes. Figure 6.6 shows a reference system $(\boldsymbol{u}_t, \boldsymbol{u}_n)$ co-moving with the S/C (tangential component points into the direction of motion), on which our investigations are based.

We assume that all thrust and lift forces lie in the $(\boldsymbol{u}_t, \boldsymbol{u}_n)$-plane. In this case the S/C moves only in this plane and our treatment is reduced to a two-dimensional case.

By assuming the Earth *reference system* to be inertial, we neglect the Earth's rotation, which leads to three errors to be considered in practice:

1. The transition to a rotating Earth reference system changes the coordinates of the S/C trajectory relative to an observer on ground.
2. The atmosphere moves with the Earth's surface, which leads to cross-components of drag and lift. They are, however, negligible compared to wind forces. Even those we do not take into account here.

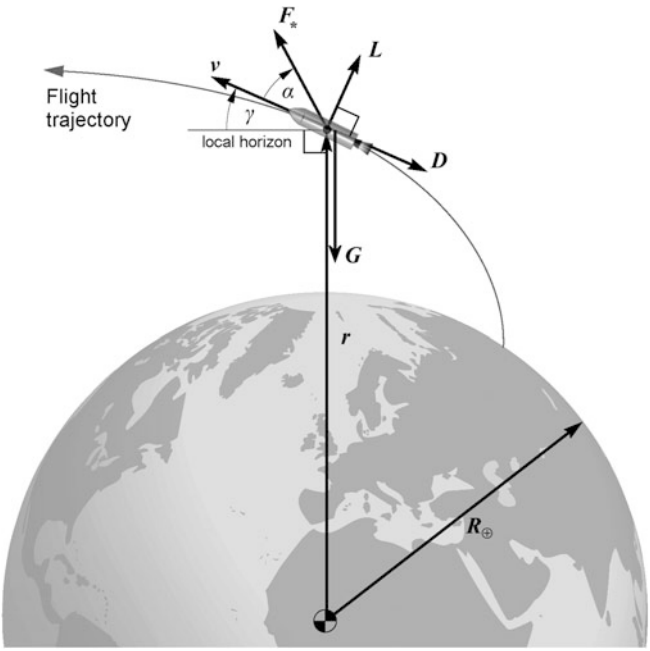

Fig. 6.8 Ascent flight of a S/C with flight path angle γ through the atmosphere subject to the effective forces: thrust F_* with thrust angle (steering angle) α, lift L, drag D, and gravitational force $G = mg$

3. At launch Earth's rotation causes a tangential velocity, which adds to the S/C velocity for a launch in the eastern direction. So placing a launch pad somewhere near the equator and launching the vehicle in an eastern direction saves propellant or alternatively enables a bigger payload. For example, the new Soyuz-2 rocket will deliver 8.5 tons of payload into LEO from Baikonur located at 45.9°N, but about 9.1 tons from Kourou at 5.1°N!

Analysis in the Co-Moving S/C System

Because lift and drag forces are conveniently defined in the $(\boldsymbol{u}_t, \boldsymbol{u}_n)$ reference system as depicted in Fig. 6.7, we will analyze the differential motion in this co-moving S/C system. The $(\boldsymbol{u}_t, \boldsymbol{u}_n)$-plane is part of the cylindrical reference system $(\boldsymbol{u}_t, \boldsymbol{u}_n, \boldsymbol{u}_h)$ with the following instantaneous unit vectors: $\boldsymbol{u}_t$ tangential to the trajectory, $\boldsymbol{u}_n$ normal to the trajectory in the motion plane (see Fig. 6.6), and $\boldsymbol{u}_h = \hat{\boldsymbol{h}}$ the vector normal to the plane equaling the angular momentum unit vector (see Sect. 7.2.2). In this reference system we have per definition

$$\boldsymbol{v} = v \cdot \boldsymbol{u}_t$$

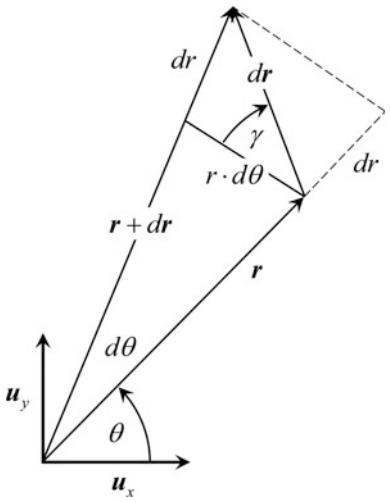

Fig. 6.9 The components of the radial vector in the inertial Earth reference system

According to Fig. 6.6 and due to a rotating $\boldsymbol{r}$ and $\boldsymbol{v}$, $(\boldsymbol{u}_t, \boldsymbol{u}_n, \boldsymbol{u}_h)$ rotates with angular velocity

$$\boldsymbol{\omega} = \left(\dot{\theta} - \dot{\gamma}\right) \cdot \boldsymbol{u}_h$$

where γ is the so-called **flight path angle**, which is the key angle in the $(\boldsymbol{u}_t, \boldsymbol{u}_n)$-system. To evaluate $\dot{\theta}$ in the $(\boldsymbol{u}_t, \boldsymbol{u}_n)$-system we derive from Fig. 6.9 $r \cdot d\theta = |d\boldsymbol{r}| \cdot \cos\gamma$. This yields (cf. Eq. (7.3.15c))

$$\dot{\theta} = \frac{v}{r}\cos\gamma \tag{6.3.2}$$

> **Note** *dr describes the change of the absolute value of the radial distance and therefore is only the radial part of the position change vector* $d\boldsymbol{r}$*, and not its value,* $dr \neq |d\boldsymbol{r}|$*, that includes the change of direction. Therefore* $v = |d\boldsymbol{r}/dt| = |\boldsymbol{v}|$ *is the absolute value of the velocity, while* $v_r = dr/dt$ *is only the radial velocity component (cf. Note in Sect. 7.2.2).*

For the acceleration vector we obtain by differentiation of $\boldsymbol{v} = v \cdot \boldsymbol{u}_t$ (see also Sect. 7.2.1)

$$\dot{\boldsymbol{v}} = \dot{v} \cdot \boldsymbol{u}_t + v \cdot \dot{\boldsymbol{u}}_t = \dot{v} \cdot \boldsymbol{u}_t + \boldsymbol{\omega} \times \boldsymbol{v}$$

With $\boldsymbol{\omega} = \left(\dot{\theta} - \dot{\gamma}\right) \cdot \boldsymbol{u}_h$, $\boldsymbol{v} = v \cdot \boldsymbol{u}_t$, and Eq. (6.3.2) we have

$$\boldsymbol{\omega} \times \boldsymbol{v} = -\left(\dot{\theta} - \dot{\gamma}\right) v \cdot \boldsymbol{u}_n = \left(\dot{\gamma} v - \frac{v^2}{r} \cos\gamma\right) \cdot \boldsymbol{u}_n \tag{6.3.3}$$

This brings us to the following form of the equation of motion

$$m\left[\dot{v} \cdot \boldsymbol{u}_t + \left(\dot{\gamma} v - \frac{v^2}{r} \cos\gamma\right) \cdot \boldsymbol{u}_n\right] = \boldsymbol{F}_* + m\boldsymbol{g} + \boldsymbol{D} + \boldsymbol{L} \tag{6.3.4}$$

Finally, we decompose the vectors on the right hand side into $\boldsymbol{u}_t, \boldsymbol{u}_n$ and obtain (cf. Fig. 6.7)

$$\begin{aligned} \boldsymbol{F}_* &= F_* \cos\alpha \cdot \boldsymbol{u}_t + F_* \sin\alpha \cdot \boldsymbol{u}_n \\ \boldsymbol{g} &= -g \sin\gamma \cdot \boldsymbol{u}_t - g \cos\gamma \cdot \boldsymbol{u}_n \\ \boldsymbol{D} &= -D \cdot \boldsymbol{u}_t \\ \boldsymbol{L} &= L \cdot \boldsymbol{u}_n \end{aligned} \tag{6.3.5}$$

where $\alpha = \angle(\boldsymbol{v}, \boldsymbol{v}_*)$ is the **thrust angle** (a.k.a. *thrust angle of attack,* which is about the **steering angle**, see Fig. 6.8), i.e., the angle between the thrust vector and the tangent to the trajectory (velocity vector). The convenience of the first and last two equations for thrust, lift, and drag forces was the reason for considering the motion in the co-moving $(\boldsymbol{u}_t, \boldsymbol{u}_n)$-system.

Scalar Equations of Motion

When inserting Eq. (6.3.5) into the vectorial equation of motion (6.3.4) the equation must hold for each component $\boldsymbol{u}_t, \boldsymbol{u}_n$ separately. In this way we derive two scalar equations of motion for a trajectory through the atmosphere:

$$\dot{v} = \frac{F_*}{m} \cos\alpha - \frac{D}{m} - g \sin\gamma \tag{6.3.6}$$

$$v\dot{\gamma} = \frac{F_*}{m} \sin\alpha + \frac{L}{m} - \left(g - \frac{v^2}{r}\right) \cos\gamma \tag{6.3.7}$$

In addition we introduce the altitude $h = r - R$ and downrange distance x, for which according to Fig. 6.9 the following holds in the Earth reference system

$$\begin{aligned} \dot{h} &= v \sin\gamma \\ \dot{x} &= v \cos\gamma \end{aligned} \tag{6.3.8}$$

We do this because this enables us to derive the time-dependent solutions $h(t)$, $x(t)$ and hence the ascent and reentry trajectory $h = h(x)$. We recall from Eqs. (6.2.23), (6.2.24), and (6.1.5) that

$$L = \frac{1}{2}\rho(r)v^2 C_L A_\perp \tag{6.3.9}$$

$$D = \frac{1}{2}\rho(r)v^2 C_D A_\perp \tag{6.3.10}$$

$$g(r) = g_0 \frac{R^2}{r^2} \tag{6.3.11}$$

$$\rho(r) = \rho_0 \exp\left(-\frac{h}{H}\right) \tag{6.3.12}$$

Here R is the radius of the celestial body in question, and $\rho_0 = 1.752\ \mathrm{kg/m^3}$ and $H = 6.7$ km are the mean barometric values for Earth as given by Eq. (6.1.6). Observe that both lift and centrifugal force (as given by the term $v^2/r \cdot \cos\gamma$) act just normal to the trajectory (see Eqs. (6.3.2) and (6.3.5)) and therefore do not show up in Eq. (6.3.6), but only in Eq. (6.3.7).

Note *Strictly speaking, the barometric formula Eq.* (6.3.12) *holds for altitudes above sea level, hence* $R =$ *sea level. Since the sea level is given by Earth's geoid (see Sect.* 12.2.1*), which roughly follows the spheriodal shape of Earth, we have* $R = R_\oplus\left(1 - 0.003353 \cdot \sin^2\beta\right)$*, where* $R_\oplus = 6378.136$ *km and* β *is the latitude.*

It is important to mention that Eqs. (6.3.6–6.3.8) implicitly require that the thrust axis coincides with the aerodynamic axis of the S/C, relative to which the thrust angle is defined, and that the center of mass lies on this axis. If this is not the case, e.g., for the Space Shuttle, then the equations of motion are far more complex, and can no longer be treated analytically. In that case one is left to solve the full equation of motion with six degrees of freedom numerically.

Only with the above form of the equation of motion it is now possible to understand flight mechanics, the science of ascent and reentry.

Normalized Equations of Motion

For studying an ascent or reentry flight in detail, the method of choice is to solve the equations of motion numerically in their time-dependent representation. Equations (6.3.6–6.3.8) are, however, not suited for that. Rather the most natural and hence optimal choice to describe the physics of nature are dimensions with unit 1. It is therefore advantageous to treat the equations of motion with dimensionless variables. In addition, such a choice makes the problem of choosing optimal spatial, time, and mass units dispensable. By defining

$$v_\triangleright = \sqrt{g_0 R}$$

and the following dimensionless variables, expressed by greek symbols

$$\mu = \frac{v}{v_\triangleright}, \quad \eta = \frac{h}{H}, \quad \chi = \frac{x}{H}, \quad \Phi = \frac{F_*}{mg_0}$$
$$\tau = \frac{g_0}{v_\triangleright}t, \quad (\ldots)' = \frac{d}{d\tau}$$

it is easy to show that the equations of motion (6.3.6), (6.3.7), and (6.3.8) can be transformed into the following normalized equations of motion

$$\begin{aligned}
\mu' &= \Phi\,\cos\alpha - \mu^2\kappa_D\tfrac{R}{H}\mathrm{e}^{-\eta} - \sin\gamma \\
\mu\gamma' &= \Phi\,\sin\alpha + \mu^2\kappa_D\tfrac{R}{H}\tfrac{L}{D}\mathrm{e}^{-\eta} - (1-\mu^2)\cos\gamma \\
\eta' &= \mu\tfrac{R}{H}\sin\gamma \\
\chi' &= \mu\tfrac{R}{H}\cos\gamma
\end{aligned}$$

normalized EoM (6.3.13)

The first three equations are coupled. This was not obvious at first glance from Eqs. (6.3.6) to (6.3.8), as both lift and drag exponentially depend on the altitude via the atmospheric density so that the ratio L/D is a constant. This is why we use L/D in the following as a convenient constant to characterize the S/C. Observe that upon ascent the thrusters are burning fuel at a high rate, which is usually about constant, $\dot{m}_p \approx const$. Therefore the S/C mass decreases almost linearly $m(t) = m_0 - \dot{m}_p t \geq m_L + m_s$, and hence

$$m(\tau) = m_0 - m'_p\tau \geq m_L + m_s \tag{6.3.14}$$

Therefore the thrust per S/C weight, $\Phi = F_*/(m(\tau)g_0)$, increases monotonically upon ascent.

The equations of motion in form of Eq. (6.3.13) are optimally adapted to be coded and solved numerically such as by a Runge-Kutta method. For specific problems more elaborate equations without the approximations made here are used. The relatively simple equations above however capture the general flight behavior, so we will limit ourselves to them.

6.4 Ascent Flight

The flight mechanics of ascent flights deals with the question of how to steer a rocket from a launch pad optimally (in terms of propulsion demand) to a predetermined target orbit. This is a very delicate task, which will lead, as we will see, to quite complex ascent strategies.

6.4.1 Ascent Phases

If you approach the problem naively from an orbit-mechanical point of view, you might consider the trajectory of the rocket as a transfer orbit between two Keplerian orbits (see Sect. 8.3) where the launch pad is a point on the initial Keplerian orbit and the target orbit is the final orbit. But of course this is not correct, as the rocket is not in a Keplerian orbit at lift-off. Nevertheless, this orbit-mechanical approach is still quite sensible. This is because, if the rocket were in a Keplerian orbit at lift-off, and if the initial aerodynamic drag at low altitudes did not occur, the solution of the problem would instantly be obvious: according to orbit mechanics, the optimal transfer orbit regarding propulsion demand is a Hohmann orbit. A Hohmann orbit is a two-impulse transfer. The first impulse carries the S/C into an elliptic transfer orbit, while the second impulse at apogee of the transfer orbit kicks it into the target orbit. Now, if we interpret the powered ascent phase as an "extended impulse maneuver" from zero velocity at lift-off to the entry of the powerless transfer orbit, we have found an important partial optimization of the ascent trajectory problem. So, we divide our optimal ascent into three phases (see Fig. 6.10):

1. **Thrust phase**—beginning with lift-off, in the thrust phase the launch vehicle traverses the atmosphere to the transition point, where thrust is terminated by the so-called MECO (main engines cut-off).
2. **Coasting phase**—starting at the transition point this phase succeeds the thrust phase. It is a powerless, weightless flight without aerodynamic drag on an elliptic transfer orbit to the target orbit.
3. **Apogee boost**—this maneuver transfers the S/C into the target orbit.

Our optimization problem has now been reduced to determining the Hohmann transfer orbital elements and the optimal trajectory in the thrust phase. Note that we hereby have presumed that the S/C is able to perform a final impulse maneuver. If this is not the case, for instance if the last stage is not reignitable, then we have a continuous thrust ascent all the way up to the target orbit. For this continuous thrust ascent problem we defer the reader to the relevant literature.

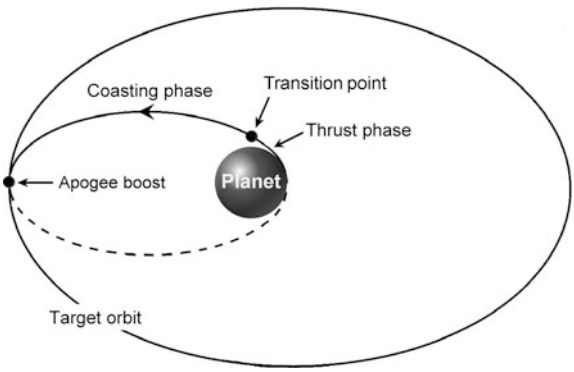

Fig. 6.10 The three ascent phases: thrust phase, coasting phase, and apogee boost

Hohmann-Transfer Orbital Elements
The orbital elements of the elliptic transfer orbit are determined on one hand by the requirement to touch the target orbit at apogee, i.e., to meet the boundary condition $r_{apo} = a_T(1 + e_T)$ (see Eq. (7.4.7)). On the other hand the transfer ellipse must touch the Earth's surface at the launch pad, i.e., $r_{per} = a_T(1 - e_T)$ (see Eq. (7.4.6)). From this follows for the two orbital elements

$$a_T = \frac{r_{apo} + r_{per}}{2}$$

$$e_T = \frac{r_{apo} - r_{per}}{r_{apo} + r_{per}}$$

Example

Let us take a Shuttle launch as an example to describe how these three phases are traversed. The launch pad at Kennedy Space Center is at sea level, so $r_{per} = 6378$ km. The target orbit typically is at an altitude of 300 km, i.e., $r_{apo} = 6678$ km. So, according to the above equations the transfer orbit has the orbital elements $a_T = 6528$ km and $e_T = 0.02298$. If the Shuttle ascended without aerodynamic drag on this ideal transfer orbit, the ascending time until reaching the target orbit would be $t_T = 43.5$ min according to Eq. (8.3.3).

Now, let us have a look at the ascent in reality. The thrust phase lasts 8.5 min, and at the transition point at an altitude of 110 km it took the Shuttle seamlessly into the transfer orbit. If the transition were not perfect, the Shuttle would, typically after 1.5 min, adjust its coasting trajectory by a so-called OMS-1 burn. Thereafter the Shuttle was in a powerless flight for 31.5 min on the elliptic transfer orbit until apogee at an altitude of 300 km. Here a so-called OMS-2 burn (apogee boost) for 2.5 min brought it into the circular target orbit. The total flight time was 42.5 min, which is just little less than the Hohmann transfer time.

Remark *Ballistic missiles after their thrust phase follow ballistic, i.e., elliptic, trajectories, which do not have their perigee at the launch pad and therefore have an additional degree of freedom, which is used to adjust the trajectory to the target distance.*

6.4.2 Optimization Problem

Having determined the transfer orbit, we are left with the final problem: Which is the optimal trajectory during the thrust phase, which smoothly transits into the

coasting phase and which consumes the least propellant? This ascent optimization problem is a typical problem of *optimal control theory* (see, e.g., Rau (2010)). Optimal control problems are inherently so complex that in general they can be solved only numerically. Here we will derive the problem setting and outline the different ascent strategies an optimal ascent is based on.

An ascent trajectory in general is determined by the equations of motion (6.3.6–6.3.8) plus the initial condition that the rocket at ignition rests on the launch-pad.

$$\begin{aligned} v(0) &= 0 \\ \gamma(0) &= 90^\circ \qquad \text{initial conditions} \\ h(0) &= h_0 \approx 0 \end{aligned} \tag{6.4.1}$$

and by the final condition that the rocket has to meet the transition point to the transfer orbit at engine cutoff. According to Eq. (10.1.4) the final condition is expressed as

$$\begin{aligned} v(t_f) &= v_f = \sqrt{\frac{\mu}{a_T\left(1-e_T^2\right)}}\sqrt{1+2e_T\cos\theta_T+e_T^2} \\ \cos\gamma(t_f) &= \cos\gamma_f = \frac{1+e_T\cos\theta_T}{\sqrt{1+2e_T\cos\theta_T+e_T^2}} \qquad \text{final conditions} \\ h(t_f) &= h_f = r_f - R = \frac{a_T\left(1-e_T^2\right)}{1+e_T\cos\theta_T} - R \end{aligned} \tag{6.4.2}$$

with t_f the time and θ_T the orbit angle where the thrust phase transfers at engine cutoff into the elliptic coasting phase. Since a_T, e_T are already determined by the transfer orbit, we only have the variables $F_*(t)$, $m(t)$, $\alpha(t)$, θ_T to find an ascent trajectory, which meets the final conditions (6.4.2). However, we also have to take into account that

$$\begin{aligned} F_* &= set \\ m(t) &= m_0 - \dot{m}_p \cdot t = set \end{aligned} \tag{6.4.3}$$

are set by thruster characteristics and the requirement that the ascent time should be as short as possible due to the gravitational loss (see Sect. 2.3.3 and below). This implies maximum thrust throughout ascent and therefore all in all thrust F_* and rocket mass m are predetermined functions of time (except temporary throttling for the Space Shuttle due to excessive drag). Therefore we only have the two variables $\alpha(t)$, θ_T to attain the optimal ascent trajectory. An optimal ascent trajectory implies that its so-called *performance index* (a.k.a. *cost functional*) *J,* which is the fuel demand, is lowest. Since the fuel demand is monotonously increasing in time and due to the gravitational loss we find the following problem setting for optimal ascent.

Formulation of the Optimal-Ascent Problem
Determine θ_T and the functional relationship $\alpha(t)$ that minimize $J = m_p(t_f)$ subject to the

1. Differential equations of ascent motion (6.3.6–6.3.8),
2. Path constraints Eq. (6.4.3), and
3. Initial and final conditions (6.4.1) and (6.4.2).

Note that the variable θ_T to be optimized can be substituted via the final condition Eqs. (6.4.2) by either v_f, γ_f or h_f.

Optimization Guidelines
Without knowing the exact solutions for $\alpha(t)$ and θ_T from numerical methods it is important to know that there are general design guidelines. To derive them we formally write $D = D(h),\ L = L(h)$, by which we indirectly include the solution of Eq. (6.3.8), so we need only to focus on the optimization treatment of the first two equations. We start this treatment by formally integrating the equation of motion (6.3.6)

$$\begin{aligned} v &= \int_0^{t_f} \frac{F_* \cos\alpha}{m} dt - \int_0^{t_f} \frac{D}{m} dt - \int_0^{t_f} g \sin\gamma \cdot dt \\ &= F_* \int_0^{t_f} \frac{dt}{m} - F_* \int_0^{t_f} \frac{1-\cos\alpha}{m} dt - \int_0^{t_f} \frac{D}{m} dt - \int_0^{t_f} g \cdot \sin\gamma \cdot dt \end{aligned}$$

from which we derive with Eq. (6.4.3), with $F_* = \dot{m}_p v_*$ (see Eq. (1.1.4)), and with Eq. (6.2.23)

$$v_f = \underbrace{v_* \ln\frac{m_0}{m_f}}_{\text{rocket equation}} \underbrace{- 2F_* \int_0^{t_f} \frac{\sin^2(\alpha/2)}{m} dt}_{\text{steering losses}} \underbrace{- \frac{1}{H} \int_0^{t_f} \kappa_D v^2 e^{-\frac{h}{H}} dt}_{\text{drag losses}} \underbrace{- \int_0^{t_f} g \sin\gamma \cdot dt}_{\text{gravitational losses}} \quad (6.4.4)$$

where κ_D is the reduced drag coefficient (see Eq. (6.2.17)). We find that there are three contributions, which reduce the velocity gain: steering losses, drag losses, and gravitational losses. Since v_f is a given final condition of the optimal-ascent problem, this equation states that reducing the target quantity m_f implies a reduction of these three velocity contributions. This is the key optimization guideline. If we were on a celestial body without any atmosphere there would not be any drag losses, so a steerless horizontal launch with $\gamma(0) = 0°$ would result in a lossless ascent. As we have an atmosphere on Earth and because rocket structures do not

support horizontal launches but only vertical ones, the initial condition is $\gamma(0) = 90°$. As we will see in Sect. 6.4.7 the loss shares of a typical ascent profile in Earth's atmosphere are: steering losses $\approx 3\%$, drag losses $\approx 27\%$, gravitational losses $\approx 70\%$. So optimal steering today is the art of reducing gravitational losses either by higher accelerations thus reducing t_f or by smaller flight path angles (early horizontal flight) at the limit of aerodynamic structural loads.

To investigate the options of affecting the flight path angle for an optimal trajectory we formally integrate Eq. (6.3.7) and find with Eq. (6.2.24)

$$\gamma_f = \frac{\pi}{2} + \underbrace{F_* \int_0^{t_f} \frac{\sin\alpha}{mv} dt}_{steering} + \underbrace{\frac{1}{H} \int_0^{t_f} \kappa_L v^2 \mathrm{e}^{-\frac{h}{H}} \cdot dt}_{lift} - \underbrace{\int_0^{t_f} \frac{g}{v} \cos\gamma \cdot dt}_{gravitation} + \underbrace{\int_0^{t_f} \frac{v}{r} \cos\gamma \cdot dt}_{centrifugal\ force} \tag{6.4.5}$$

where κ_L is the reduced lift coefficient (see Eq. (6.2.18)). Note that these terms do not imply losses. They just change the flight path angle. From this follows the secondary optimization guideline to make use of steering, lift, gravitation, and centrifugal to shape the flight path such that the steering, drag, and gravitational losses are minimized.

Optimal-Ascent Considerations

With Eqs. (6.4.4) and (6.4.5) at hand we are able to ponder about an optimum-ascent trajectory. Taking all the contributions adequately into account is quite an engineering feat, and we are not able to discuss it extensively in this book. However, we want to capture at least the essential aspects of optimization.

During the thrust phase the spacecraft changes its state vector from a vertical launch direction, $\gamma_i = \pi/2$, with zero initial velocity to a nearly horizontal flight direction, $\gamma_f = 0$, and maximum velocity at engine shutdown at the transition point. We first want to investigate the losses due to velocity direction changes. Two direction changes have to be taken into consideration: the turn into the desired target-orbit inclination, and the turn from the vertical launch direction into the incline of the transfer orbit.

As long as the S/C ascents vertically the turn into the so-called launch azimuth (angle between geographic north and the orbit trajectory, see Sect. 8.6.1) is just a tilt of the axially symmetric rocket into this direction or a roll of an asymmetrical S/C along its vertical axis into the launch azimuth. Let us take the Space Shuttle as an example for the latter. Because the launch pad at Kennedy Space Center is oriented roughly southward, which is a remnant of the Apollo era, the Shuttle first had to roll by 120° around its longitudinal axis to match its body symmetry plane (x-z plane) with the orbital plane of the International Space Station. This was the famous 120° roll maneuver. The losses due to such tilt or roll maneuvers of course can be neglected.

Concerning the turn from the vertical launch direction into the incline of the transfer orbit there and according to Eq. (6.4.5) there are four effects which contribute to a changing flight path angle: steering, lift, gravitation, and centrifugal force. The positive sign of the centrifugal term in Eq. (6.4.5) indicates that this a countering effect we have to live with. Of course, flight angle reduction can be achieved by a negative steering angle $\alpha < 0$. However, any steering brings about steering losses, which need to be kept as small as possible. If the body of the S/C is not axially symmetric, such as the winged body of the Space Shuttle, it generates lift, which can be harnessed to reduce the flight path angle more quickly by turning the Shuttle upside down ($\kappa_L \rightarrow -\kappa_L$), which actually was done. So lift can be looked at as a kind of additional steering option, which we will neglect in the following because most rockets have no lift because they are built symmetrically.

What is the least fuel consumption trajectory into space? Equation (6.4.4) with (6.4.5) claim that flight path angle reduction is most effective if high steering angles are applied at low speeds, i.e., just after lift-off. A small γ early on would also reduce the gravitational loss term $g \sin\gamma$. But you do not want to turn too early, because drag is very high at low altitudes (see exponential contribution in drag term in Eq. (6.4.4)). Because steering losses contribute with only about 3% to the total ascent losses, the optimal-ascent problem hence seems to be a matter of trading drag losses against gravitational losses and that there is a wide range of possible trajectories into space due to these contradictory requirements. Yet this is not the case because there is gravity turn.

6.4.3 *Gravity Turn*

Why wasting propellant to steer the rocket into horizontal flight when gravity does it for you?

According to Eq. (6.4.5) gravity reduces the flight path angle without any steering. It is like throwing a stone forward and upward. Gravity bends its trajectory until it flies horizontally at its apex. Now, accelerate the stone in flight, which will shift the apex into space and the increasing centrifugal force will prevent it from falling back. Thus you have the gravity turn of an ascending rocket. Since the required thrust angle is $\alpha = 0$, there are no steering losses for the velocity gain (second term in Eq. (6.4.4)). Mathematically the gravity turn maneuver can be described by setting $\alpha = 0$ in Eq. (6.3.7) and neglecting lift. We then get for the flight path angle rate

$$\dot{\gamma} = -\left(\frac{g}{v} - \frac{v}{r}\right)\cos\gamma \tag{6.4.6}$$

We see that the initial rate and hence the gravity turn is big at low speeds (but zero for vertical ascent). With rising altitudes, velocity increases, so gravity turn

Fig. 6.11 Ascent trajectory with gravity turn until main engines cut-off (MECO) of an ascending Delta II rocket from Vandenberg Air Force Base on July 2, 2014. *Credit* Rick Baldridge

diminishes while centrifugal forces become stronger until $g/v - v/r = 0 \rightarrow v \approx \sqrt{gR} = 7.92$ km s^{-1}. When this happens $\dot{\gamma} \approx 0$, and if the gravity turn was initiated just right, also $\gamma \approx 0°$, i.e., the trajectory is nearly circular at the transit point. This can somehow be gleaned from the image of an ascending rocket at night in Fig. 6.11. The gravity-turn ascent is equivalent to the opposite case of a ballistic entry as discussed in the Sect. 10.3.2.

You might think that gravity turn is the philosopher's stone for ascent. This is not the case, because a gravity-turn-only ascent just eliminates steering losses. But, as we will see in Sect. 6.4.7, drag and gravity losses are one order of magnitude more significant than steering losses, which are not minimal for such an ascent. So, although an optimized ascent is close to a gravity-turn ascent it needs some additional ingredients. Moreover, with vertical lift-off a gravity turn does no happen all by itself. It needs to be kicked off.

6.4.4 Pitch Maneuver

For structural reasons, the S/C is in a vertical position at lift-off. So just after lift-off the flight path angle is $\gamma = 90°$, $\alpha = 0$ and $L = D = 0$. From Eq. (6.4.6), we get $\dot{\gamma} = 0$: the S/C will ascent vertically. In order to subject it to a gravity turn, we need a so-called *initial kick angle* (a.k.a. *pitch angle*, i.e., the angle between flight direction and the vertical), which may be small, but not zero. This pitch angle is brought about by the so-called *pitch maneuver* or *pitch program*, and it amounts to approximately 3–5° (see Fig. 6.12). Only after receiving the kick angle the pitch will increase further due to the gravitational force according to Eq. (6.4.6) until it acquires about 20–30° at an altitude of 10–15 km. Note that for small celestial bodies without any atmosphere a timely pitch maneuver plus a gravity turn together

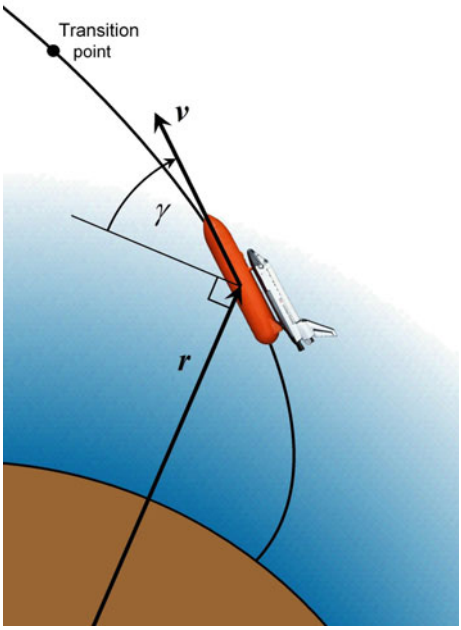

Fig. 6.12 Pitch maneuver and constant pitch-rate maneuver just after lift-off

make up an optimal ascent. So the ascent of the Apollo landing module from the Moon was virtually an ideal pitch and gravity turn.

6.4.5 Constant-Pitch-Rate Maneuver

How are drag losses minimized? According to Eq. (6.3.10) drag is small, if at low altitudes, despite a high atmospheric density, the velocity is very low. This is always the case after lift-off. But flight velocity increases rapidly, so the maximum aerodynamic pressure, so-called $q_{\max}$ (a.k.a. *max q*), is achieved at medium altitudes, and it may become quite big. At increasing altitudes, aerodynamic pressure decreases due to the exponential decline of the atmospheric density with altitude. Apart from substantial drag losses, aerodynamic pressure also puts on high dynamic loads. This is why at max q the Space Shuttle temporarily throttled down its three liquid propulsion engines to about 70% thrust (see Fig. 6.1). So from the sole perspective of drag losses, the ascent should be as slow as possible and with the shortest trajectory through the atmosphere (Fig. 6.13).

To account for this requirement the so-called constant pitch rate (CPR) maneuver is frequently used rather than the gravity turn. The **pitch angle** is defined as $\theta := \alpha + \gamma$. A CPR would therefore imply $\dot{\theta} = \dot{\alpha} + \dot{\gamma} = const < 0$. We want to know, how the vehicle needs to be steered, i.e., how $\alpha(t)$ looks like just after lift-off, to achieve a constant pitch rate. This problem is closely related to the

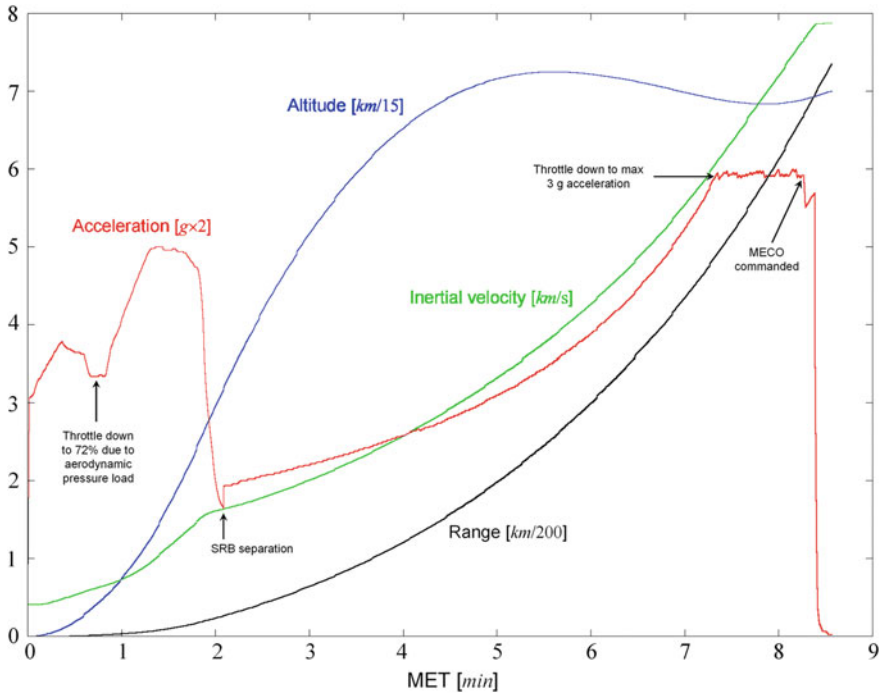

Fig. 6.13 A typical Space Shuttle ascent profile (here STS-122). MET (mission elapsed time) = time from lift-off, SRB = solid rocket booster, MECO = main engine cut-off. Observe that due to Earth's rotational velocity the inertial velocity of the Shuttle was not zero at lift-off. An overshoot in altitude is typical for any spacecraft ascent, which is due to the necessity of a longer vertical flight to reduce aerodynamic resistance rather than to obey an optimal gravity turn

problem, what the steering after lift-off is for a constant flight path angle rate (CFPAR), $\dot{\gamma} = const < 0$. We first investigate the latter problem before we come to the CPR problem.

Constant Flight Path Angle Rate

After lift-off we are at low speed, so we can neglect drag, lift, and centrifugal forces. In this case the flight path angle would decrease according to $\gamma = 90^\circ + \dot{\gamma} t$ with $\dot{\gamma} = const < 0$. We get from Eq. (6.3.7)

$$\begin{aligned} v\dot{\gamma} &= \frac{F_*}{m}\sin\alpha - g\,\cos\gamma = a_*\sin\alpha - g\,\cos\gamma \\ F_* &=: ma_* \end{aligned} \tag{6.4.7}$$

where we have defined the thrust acceleration a_*. In order to derive $\alpha(t)$ and with $\gamma(t) = set$ we need to find an expression for v. Considering Eq. (6.3.6), we find for $D \ll F_*$ and because thrust angles are always small

$$\dot{v} = a_* \cos\alpha - g\,\sin\gamma \approx a_* - g\,\sin\gamma$$

We integrate both sides with regard to time. With $m(t) = m_0 + \dot{m}t$ from Eq. (6.4.3) and with $v(t=0) = v_0$ and the condition $\dot{\gamma} = const$, we find

$$\begin{aligned} v - v_0 &= \int_0^t \frac{F_*}{m_0 + \dot{m}t'}dt' - g\int_{90^\circ}^{\gamma} \frac{\sin\gamma'}{\dot{\gamma}}\cdot d\gamma' = a_{*0}\int_0^t \frac{dt'}{1 + \dot{m}t'/m_0} - \frac{g}{\dot{\gamma}}\int_{90^\circ}^{\gamma} \sin\gamma'\cdot d\gamma' \\ &= a_*\frac{m}{\dot{m}}\ln\left(1 + \frac{\dot{m}}{m_0}t\right) + \frac{g}{\dot{\gamma}}\cos\gamma \end{aligned}$$

Inserting this into Eq. (6.4.7) yields

$$\dot{\gamma}\left[a_*\frac{m}{\dot{m}}\ln\left(1 + \frac{\dot{m}}{m_0}t\right) + v_0\right] + g\,\cos\gamma = a_*\sin\alpha - g\,\cos\gamma$$

As $\gamma = 90^\circ + \dot{\gamma}t$, $\cos\gamma = -\sin\dot{\gamma}t$, so we finally obtain for the thrust angle to steer a constant FPA rate

$$\sin\alpha(t) = \dot{\gamma}\left[\frac{m}{\dot{m}}\ln\left(1 + \frac{\dot{m}}{m_0}t\right) + \frac{mv_0}{F_*}\right] - 2\frac{mg}{F_*}\sin\dot{\gamma}t \qquad \textbf{CFPAR steering law} \tag{6.4.8}$$

This law applies whenever $D, L \ll F_* = const$, $\dot{\gamma} = const$, and v small. After lift-off, when $\dot{\gamma}\,t \ll 1$ and $\dot{m}t \ll m_0$, that is, $m \approx m_0$, we derive the approximate result

$$\sin\alpha(t) \approx \alpha(t) \approx \dot{\gamma}\left[t\left(1 - 2\frac{m_0 g}{F_*}\right) + \frac{m_0 v_0}{F_*}\right] \tag{6.4.9}$$

So the thrust angle increases linearly with time.

Note *In the special case $F_* = 2m_0 g$, that is, if the thrust is twice as much as the weight of the vehicle, the thrust angle to steer $\dot{\gamma} = const$ becomes constant, and zero for $v_0 = 0$. This means that in a drag-free and lift-free initial stage of ascent where $\dot{m}t \ll 2m_0$ and $\dot{\gamma}^2 t^2 \ll 6$ the gravity turn alone does the job.*

Constant Pitch Rate

We now turn back to the CPR problem. Since the flight path angle rate depends on the steering angle, $\dot{\gamma}(\alpha)$ (see Eq. (6.3.7)), we have with $\dot{\alpha} + \dot{\gamma}(\alpha) = \dot{\theta} = const$. This is a differential equation for $\alpha(t)$, which however is too complex to be solved analytically. But we can simplify this problem by making the special choice $\dot{\gamma} = const$, i.e., applying the CFPAR steering law. From $\dot{\alpha} = \dot{\theta} - \dot{\gamma} = const$ follows that

$$\alpha(t) = \left(\dot{\theta} - \dot{\gamma}\right) t + \alpha_0$$

Solving Eq. (6.4.9) for $\dot{\gamma}$ and inserting it yields

$$\alpha \frac{2 - 2g/a_{*0}}{1 - 2g/a_{*0}} = \dot{\theta}\, t + \frac{v_0 \dot{\gamma}/a_{*0}}{1 - 2g/a_{*0}} + \alpha_0$$

from which we finally obtain

$$\alpha(t) = \frac{a_*/2 - g}{a_* - g}\left(\dot{\theta} t + \alpha_0\right) + \frac{1}{2}\frac{v_0 \dot{\gamma}}{a_* - g} \qquad \begin{array}{l}\textbf{linear CPR steering law} \\ @\ \dot{\gamma} = const\end{array} \tag{6.4.10}$$

Here, as well, we find that, if $a_* = 2g$ then $\alpha(t) = const$ and no steering is needed. For $v_0 = 0$ there are even no steering losses.

6.4.6 Terminal State Control

The terminal state control problem considers the case where the ascending vehicle initially is in the state $(\boldsymbol{r}(t_i), \boldsymbol{v}(t_i)) =: (\boldsymbol{r}_i, \boldsymbol{v}_i)$ and targets the final state $\left(\boldsymbol{r}(t_f), \boldsymbol{v}(t_f)\right) =: \left(\boldsymbol{r}_f, \boldsymbol{v}_f\right)$, which for instance is given by Eq. (6.4.2). So, this is exactly the control we need to solve the optimization problem as described in Sect. 6.4.2. However, it can be shown that there exists no analytical solution if aerodynamic forces act on the vehicle. We therefore turn to the simpler case at high altitudes where we have no aerodynamic forces. In this case the master Eq. (6.3.1) reduces to the equations of motion

$$\begin{aligned} \dot{\boldsymbol{r}} &= \boldsymbol{v} = \begin{pmatrix} v_x \\ v_y \end{pmatrix}_{RSW} \\ \dot{\boldsymbol{v}} &= \boldsymbol{a}_* + \boldsymbol{g} = \begin{pmatrix} a_* \cos(\alpha + \gamma) \\ a_* \sin(\alpha + \gamma) - g \end{pmatrix}_{RSW} \end{aligned} \qquad @\ \text{no aerodynamic forces}$$

where

$$\boldsymbol{a}_* = \frac{\boldsymbol{F}_*}{m} = a_* \begin{pmatrix} \cos\alpha \\ \sin\alpha \end{pmatrix}_{NTW} = a_* \begin{pmatrix} \cos(\alpha + \gamma) \\ \sin(\alpha + \gamma) \end{pmatrix}_{RSW}$$

is the thrust acceleration expressed in the *NTW* and *RSW* Cartesian topocentric satellite coordinate systems co-moving with the vehicle (see Sect. 13.1.4).

Optimal Performance Control

Let us assume that by means of an optimization technique we have found a $\gamma(t)$ and t_f that maximizes the performance index J, that is the total vehicle mass at the target point. Owing to $m(t_f) = m_0 - \dot{m}_p \cdot t_f = m_0 - m_p(t_f)$ this is equivalent to

minimizing the expended propellant or to minimizing t_f. Then it can be shown by variational calculus (see e.g. Battin (1987, p. 562ff)) that in the case of absent aerodynamic forces one gets, in the most general case, a bilinear tangent steering law for $\alpha(t)$

$$\tan[\alpha(t)+\gamma(t)] = \frac{c_1(t_f - t) + c_2}{c_1'(t_f - t) + c_2'} \quad \textbf{bilinear tangent steering law}$$

where the constants c_1, c_2, c_1', c_2' are given by the constraint that the initial $(\boldsymbol{r}_i, \boldsymbol{v}_i)$ and final $(\boldsymbol{r}_f, \boldsymbol{v}_f)$ state satisfy the corresponding boundary conditions. Even more generally it was shown that the bilinear tangent steering law is independent of the optimization function.

Furthermore, if the terminal downrange distance is unconstrained, which is the case when one just needs to get into an Earth orbit, as assumed above in Eq. (6.4.2), then it can be shown that $c_1' = 0$ and the bilinear tangent steering law reduces to the linear tangent steering law

$$\tan[\alpha(t)+\gamma(t)] = a(t_f - t) + b \quad \textbf{linear tangent steering law}$$

Employing the initial and terminal boundary conditions leads to

$$\tan[\alpha(t)+\gamma(t)] = \tan(\alpha_i+\gamma_i) - \left[\tan(\alpha_i+\gamma_i) - \tan(\gamma_f)\right]\frac{t}{t_f}$$

If Earth is assumed to be flat, the *RSW* coordinate system is a Cartesian system, where *x,y* span the flight plane and *y* points up vertically. The terminal velocity vector then can be written (see Eq. (6.4.2)) as

$$\boldsymbol{v}_f = \begin{pmatrix} v_x(t_f) \\ v_y(t_f) \end{pmatrix}_{x,y} = v_f \begin{pmatrix} \cos\gamma_f \\ \sin\gamma_f \end{pmatrix}_{x,y} = \sqrt{\frac{\mu}{a_T(1-e_T^2)}} \begin{pmatrix} 1 + e_T\cos\theta_T \\ e_T\sin\theta_T \end{pmatrix}_{x,y}$$

With this, the following linear tangent steering law can be shown (Battin 1987, p. 565) to be optimal

$$\tan[\alpha(t)+\gamma(t)] = \frac{g\cdot(t_f - t) + v_y(t_f)}{v_x(t_f)} \tag{6.4.11}$$

Note that at the transition point, when $t = t_f$, we have $\tan(\alpha+\gamma) = v_y(t_f)/v_x(t_f) = \tan\gamma$ and hence the steering angle becomes $\alpha(t_f) = 0$.

It must be emphasized that a tangent steering law does not optimize the performance index *J*. Rather, a numerical optimization method, not discussed here, that obeys the initial and final boundary conditions and the qualitative characteristics as discussed in Sects. 6.4.2–6.4.5 delivers $\gamma(t)$ and the duration t_f for the optimal

trajectory of the powered flight. A linear or bilinear tangent steering law is just the means to provide the corresponding steering $\alpha(t)$ for this optimal trajectory.

A key point of terminal state control is that the resulting linear tangent steering law is linear in time. The other is that the steering at any point in time is independent of the history of the thrust acceleration in the thrust phase.

It can be shown that the linear tangent steering is continuous even when the thrust magnitude becomes zero or switches instantaneously between zero and maximum thrust magnitude. This is a perfect criterion for today's thermal thrusters, which most effectively work in a pulsed rather than in a throttling mode. Steering control that makes use of this pulsed acceleration is called *bang-bang control*. Therefore bang-bang profiles are often used for linear tangent steering.

All these advantages enables the linear tangent steering law to be applied as a single steering law through all rocket stages regardless of their variations of thrust and propellant flow rates. It is this universality and simplicity why it is commonly used as an approximate steering law in realistic ascent problems, in particular at high altitudes where the aerodynamic forces become negligible.

6.4.7 Optimal Ascent Trajectory

In summary, the following qualitative picture of an optimal ascent can be given: Immediately after vertical lift-off the S/C is rolled if required (Space Shuttle) into the target orbit inclination. It is then subjected to a pitch and constant pitch rate maneuver which requires only a low propulsion demand at these low speeds. This brings the S/C in a relatively steep trajectory to altitudes where drag has reduced to a level that a loss-free gravity turn bends the trajectory more and more horizontally. The cross-over from constant pitch rate with $\alpha \neq 0$ to gravity turn with $\alpha = 0$ of course is steady. Detailed investigations have shown that a good approximation to the ideal thrust phase trajectory is the following approach:

1. At altitudes below roughly 25 km a piecewise constant thrust angle rate profile of the empirical form

$$\dot{\alpha} = \dot{\gamma} \cdot \mathrm{e}^{-\kappa t} \tag{6.4.12}$$

   is chosen with form factors $\dot{\gamma}$, κ to be determined as part of the overall optimization. In this region of high dynamic pressure near zero steering angles are flown to reduce bending loads caused by wind shear.
2. At altitudes above 25 km a closed-loop guidance based on bilinear or linear tangent steering law is usually initiated, in which real-time integration of the dynamic equations of motion is performed to determine the value of the guidance parameters that meet the desired terminal conditions.

Since we have seen that for bilinear and linear tangent steering $\alpha(t_f) = 0$, at the end of the thrust phase the ascent trajectory passes smoothly into the elliptic transfer orbit, which finally touches and transits into the target orbit.

For such an optimized ascent trajectory the extra delta-v for an ascent into a low Earth orbit are typically:

- Steering $\Delta v \approx 0.05$ km s^{-1}
- Drag $\Delta v \approx 0.4$ km s^{-1}
- Gravitation $\Delta v \approx 1.0$ km s^{-1}
- Earth's rotation $\Delta v = -0.464 \cdot \cos\beta$ [km s^{-1}].

Earth's rotation Δv is the surface speed of the launch pad at latitude β due to the rotation of the Earth, which directly adds to the total delta-v as a negative (for a prograde orbit) contribution. In total, the delta-v budget for a typical 250 km parking orbit is

$$\begin{aligned}\Delta v_{tot} &= 7.75 + 0.05 + 0.4 + 1.0 - 0.464 \cdot \cos\beta \left[\text{km s}^{-1}\right] \\ &= 9.2 - 0.464 \cdot \cos\beta \left[\text{km s}^{-1}\right]\end{aligned}$$

So, as a rule of thumb the delta-v required to get into LEO from a low latitude launch pad (such as Kennedy Space Center) including a typical margin of about 0.3 km/s is $\Delta v_{tot} \approx 9$ km/s.

To determine an optimal-ascent trajectory with such optimized losses, for instance by determining the form factors $\dot{\gamma}$, κ, is a brilliant feat, in particular when also staging, variations in thrust, aerodynamic properties of the vehicle and winds are taken into account. In the end, a good ascent optimization is based on sophisticated software, on the knowledge of the basic ascent maneuvers, but also a lot on the skills of experienced flight mechanics engineers and on trial and error.